



<b>FCH JU Grant Agreement no.:</b>	<b>245113</b>
<b>Project acronym:</b>	KEEPPEMALIVE
<b>Project title:</b>	Knowledge to Enhance the Endurance of PEM fuel cells by Accelerated Lifetime Verification Experiments
<b>Funding scheme:</b>	Collaborative Project
<b>Area:</b>	SP1-JTI-FCH.3 Stationary Power Generation & CHP
<b>Start date of project:</b>	01.01.2010
<b>Duration:</b>	42 months
<b>Project Coordinator:</b>	SINTEF (NO)

<b>Author (partner):</b>	Thor Anders Aarhaug (SINTEF)
<b>Other authors:</b>	Laila Grahl-Madsen (IRD); Thor A. Aarhaug (SINTEF); Ann M. Svensson (SINTEF); Luis Colmenares (SINTEF); Steffen Møller-Holst(SINTEF)
<b>Work package:</b>	WP5, Design and evaluation of experiments
<b>Work package leader (partner):</b>	Thor Anders Aarhaug (SINTEF)
<b>Date released by WP leader:</b>	2012-08-20
<b>Date released by Coordinator:</b>	2012-08-31

Dissemination level		
PU	Public	X
PP	Restricted to other programme participants (including the Commission Services)	
RE	Restricted to a group specified by the consortium (including the Commission Services)	
CO	Confidential, only for members of the consortium (including the Commission Services)	

Revisions			
Version:	Date:	Changed by:	Comments:
0.10	2012-03-15	Laila Grahl-Madsen	Input on $\mu$ CHP field experience
0.20	2012-06-18	Laila Grahl-Madsen	Report update to make the report public
0.30	2012-06-21	Thor Aarhaug	Draft TOC for report
0.40	2012-06-28	Thor Aarhaug	TAA input to IRD data
0.50	2012-06-29	Thor Aarhaug	Inclusion of modelling section
0.90	2012-08-20	Thor Aarhaug	Inclusion of gas analysis data, formatting
0.95	2012-08-21	Luis Colmenares	Inclusion of ECSA measurements
1.00	2012-08-31	Steffen Møller-Holst	Restructured and final review

## Table of Contents

<b>1</b>	<b>Real-life Experience with Hydrogen Fuelled <math>\mu</math>CHP units</b> .....	<b>3</b>
1.1	Introduction .....	3
1.2	Field Experience from Vestenskov 2010-2012 .....	3
1.3	Results and Discussion .....	5
1.4	Conclusions from real life field tests .....	13
<b>2</b>	<b>Results and experiences from phase 1 of Accelerated Stress Tests</b> .....	<b>14</b>
2.1	Introduction .....	14
2.2	Challenges encountered in phase 1 of the AST program .....	14
2.2.1	Inter-laboratory variance .....	14
2.2.2	Standard deviation and unstable operation .....	15
2.2.3	Break-in procedure not adequate for new, improved membrane materials .....	16
2.2.4	Implications for the interpretation of AST results .....	16
2.3	Findings from individual AST protocols .....	17
2.3.1	Interpretation of results from Continuous Operation AST protocol .....	17
2.3.2	Interpretation of results from Fuel Starvation AST protocol .....	18
2.3.3	Other AST protocols with insufficient data for statistical analyses .....	29
	<i>Reformate operation</i> .....	29
	<i>Dead-End operation</i> .....	29
	<i>Start-Stop Cycling</i> .....	29
	<i>Load Cycling</i> .....	29
2.4	Summary and conclusions on main factors causing degradation .....	30
<b>3</b>	<b>Modelling of <i>ex-situ</i> catalyst degradation</b> .....	<b>31</b>
3.1	Introduction .....	31
3.2	Experimental conditions and results from catalyst degradation experiments .....	31
3.3	Mathematical model .....	32
3.4	Adaption of the mathematical model to the experimental results .....	33
3.5	Conclusion .....	36
<b>4</b>	<b>Input to revision of the AST program</b> .....	<b>37</b>
<b>5</b>	<b>Abbreviations</b> .....	<b>38</b>

# 1 Real-life Experience with Hydrogen Fuelled $\mu$ CHP units

## 1.1 Introduction

The Danish micro combined heat and power ( $\mu$ CHP<sup>1</sup>) project<sup>2 & 3</sup> develops and tests fuel cells integrated into units for single family houses. The project is outlined in the KeePEMalive delivery report D1.1<sup>4</sup>. The aim of the present section is to elaborate on the field experience gained during phase three (3) of the demonstration project in Vestenskov village. The hydrogen fuelled low temperature proton exchange membrane fuel cell (LT PEMFC) field test comprises 35  $\mu$ CHP units. The stacks contain 47 cells and the operation is controlled by the heat demand in the house. In phase three (3) the  $\mu$ CHP was designed and CE-certified prior to the field test that was initiated with one unit in November 2010.

## 1.2 Field Experience from Vestenskov 2010-2012

The two first units put into operation at Vestenskov were based on an old MEA design and stack technology. They were operated for 875 and 350 hours respectively, before the MEAs developed crossover. Post-mortem analyses showed that the crossover occurred at the hydrogen inlet. The crossover is believed to be caused mainly by a combination of dry-hydrogen operation (dehydration), aggravated by idle-mode high cell voltages, presumably leading to membrane thinning. A deeper failure analysis that included data-logging in the idle-mode periods showed that the balanced air ventilation allows air-flow through the stack during windy periods, resulting in longer periods with OCV-conditions (Figure 1).

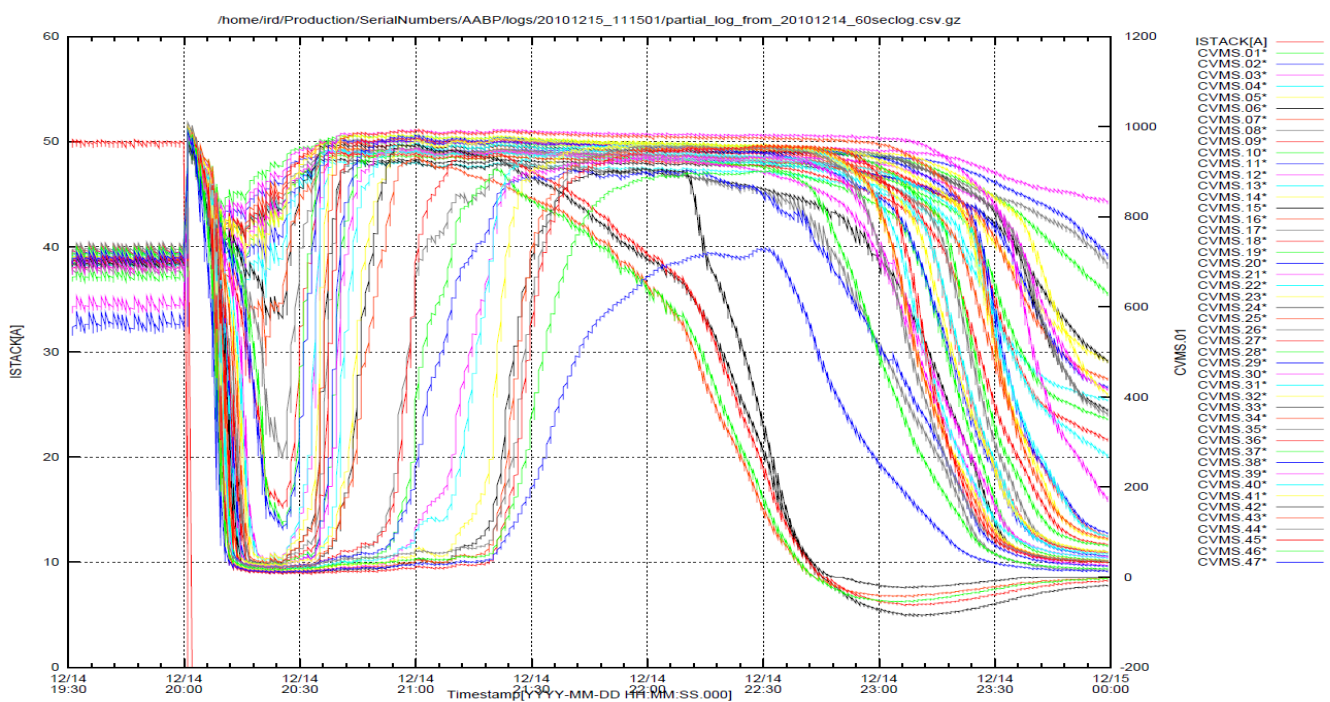


**Figure 1. Individual cell voltages observed in a stack at the field test in Vestenskov. As the load (50A) is switched off, cell voltages drop initially. Due to wind exposure to the cathode side, OCV is observed on most of the cells.**

<sup>1</sup> Abbreviations are listed in Chapter 5

<sup>2</sup> Partly funded by Energinet.dk (phase 1) and The Danish Energy Agency (phase 2 & 3) through the contracts: PSO J.no. 2006-1-6295, and EFP-Akt.167 J.no. 033001/33033-0151, respectively

<sup>3</sup> Further information can be found at <http://www.dk-mchp.eu/project.html>

<sup>4</sup> Grahl-Madsen, L et al. (2010): Overview of real-life operation conditions. KeePEMalive delivery report D1.1, 29 p.

The analysis also pin-pointed non-ideal hydrogen control during the start-up situation and degradation due to the use of dry hydrogen. The variation in the individual cell voltages (secondary y-axis) shown in Figure 1 is related to the specific (non-optimal) stack design. The cells of lower numbering are more exposed to wind, thus responding more quickly. Negative cell voltages are also observed for some cells. The voltage reversal can be explained by residual current in the stack, where some cells in the absence of oxygen will operate in a hydrogen pumping mode. This condition is not expected to be degrading the stack.

IRD therefore took the following initiatives to improve the stack design:

1. One unit ( $\mu$ CHP020) was solely equipped with an improved hydrogen supply system that ensured hydrogen humidification and prevented fuel starvation. To ensure that the effect of the improved hydrogen control could be verified, a unit had MEAs based on the fragile Nafion 212 membrane was chosen (Figure 2).
2. Another unit ( $\mu$ CHP018) was equipped with MEAs based on reinforced Nafion XL100 membranes, solely (Figure 4). The test is *on-going*.
3. A third unit ( $\mu$ CHP013) was equipped with an air-check valve to prevent idle-mode OCV voltages; and MEAs based on reinforced Nafion XL100 membrane (Figure 7). The test is *on-going*.
4. A fourth unit was equipped with an air-check valve to prevent idle-mode OCV voltages; MEAs based on reinforced Nafion XL100 membrane, and the improved hydrogen supply system design. This test has just begun and will not be mentioned any further.

The results are summarised in Table 1. The longer stop period for both  $\mu$ CHP013 and  $\mu$ CHP018 was caused by a frozen hydrogen exhaust pipe.

**Table 1. Summary of results with for three hydrogen fuelled  $\mu$ CHP units as part of the Vestenskov field test. All membranes are Nafion type (XL and 212, respectively).**

Unit	Membrane	Hours since start	Operational hours	Stack power produced [MWh]	Overall decay rate $\mu$ V/h	No. start/stop	kWh <sub>DC</sub> per cm <sup>2</sup> MEA
$\mu$ CHP013	XL	5,323	3,455	5.47	-4	783	0.75
$\mu$ CHP018	XL	6,271	4,432	7.03	-24	771	0.96
$\mu$ CHP020	212	2,666	2,240	3.64	-19	127	0.50

### 1.3 Results and Discussion

All initiatives taken to improve system design have proven to extend the MEA life-time significantly. The MEAs in the unit equipped with the improved hydrogen control [ $\mu$ CHP020, Figure 2] proved more than twice as long lifetime as previously experienced. The MEAs developed crossover after 2,240 operational hours. Post mortem analysis showed that the crossover was developed underneath the GDL in the first 1/3 of the hydrogen flow field. This is in contrast to the situation (and frequency) of pin-holes developed in MEAs tested in  $\mu$ CHP-units without the improved control (see Figure 3). These improvements had therefore enhanced the lifetime.

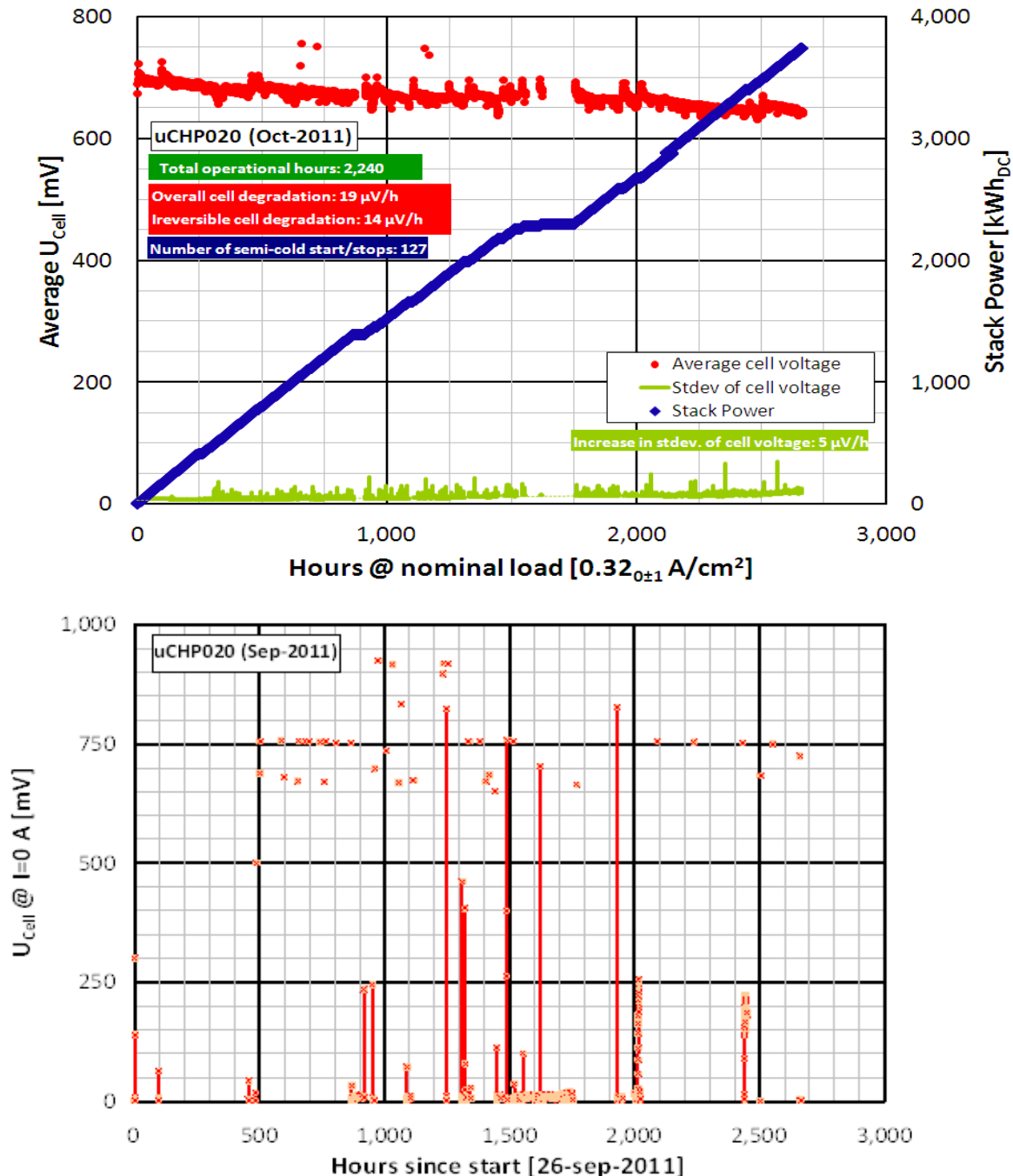
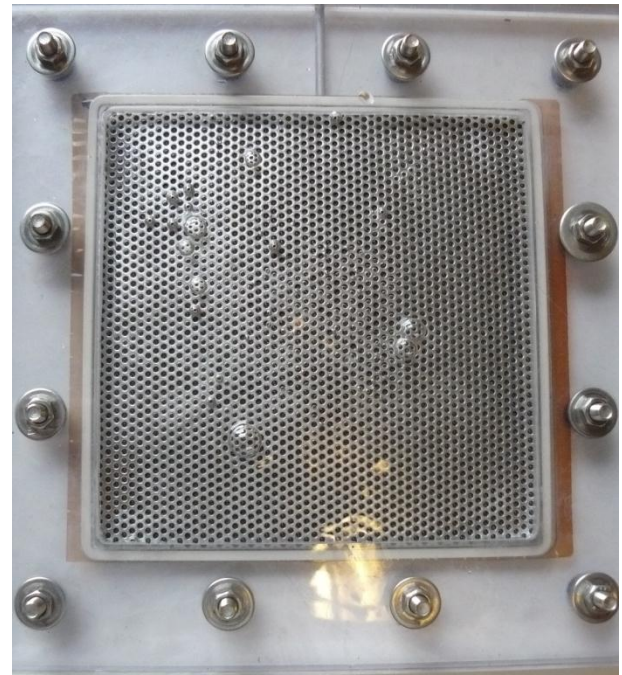


**Figure 2.** Results of the field test with unit  $\mu$ CHP020; *above*) average cell voltage [mV] and accumulated stack energy output [MWh<sub>DC</sub>]; *below*) Cell voltages during idle-mode conditions (this test was done in IRDs laboratories and the cells were therefore not exposed to long-time OCV conditions).



**A.**



**B.**

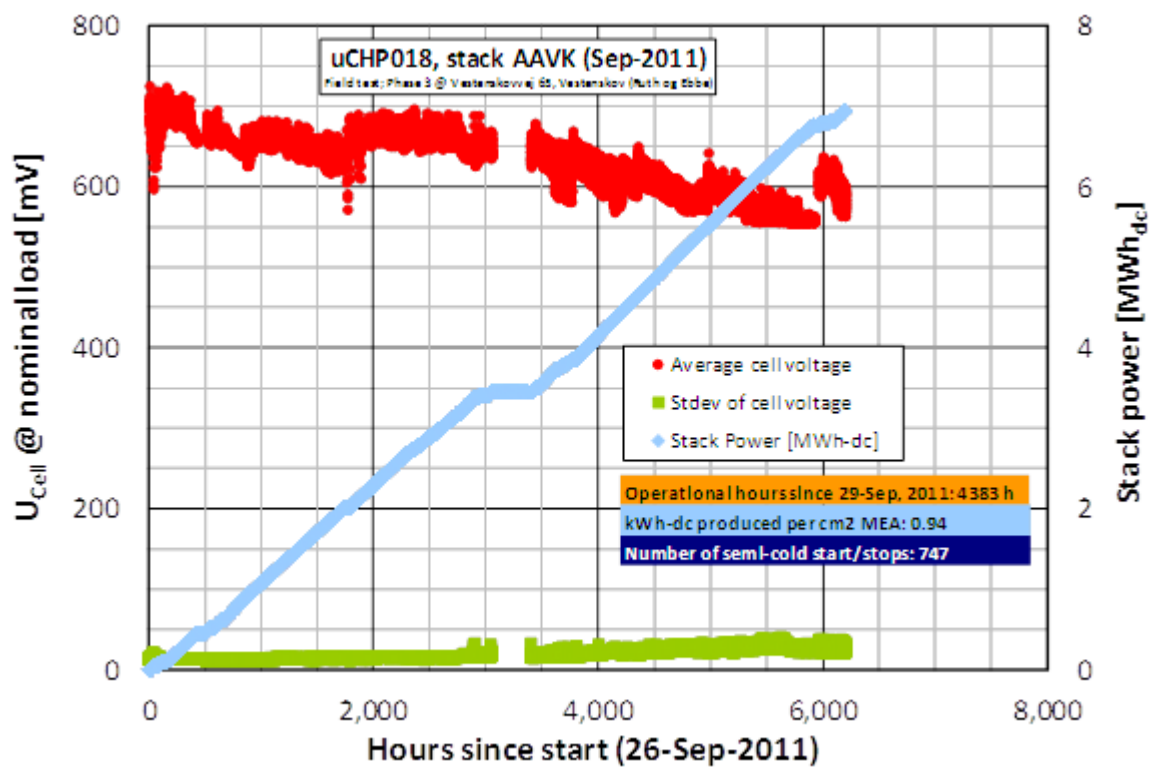
**Figure 3. Simplified test for visual inspection of pin-hole location in a failed MEA with the hydrogen inlet in the upper left corner. The MEA is fixed in a frame with a perforated plate on top (12.5\*12.5 cm) and exposed to air underneath and water on top. Air bobbles going through the MEA locate the position of the pin-holes.**

**A (left): Typical pin-holes developed in MEAs tested in  $\mu$ CHP-units before the hydrogen control was improved. The shown MEA is based on Nafion 212.**

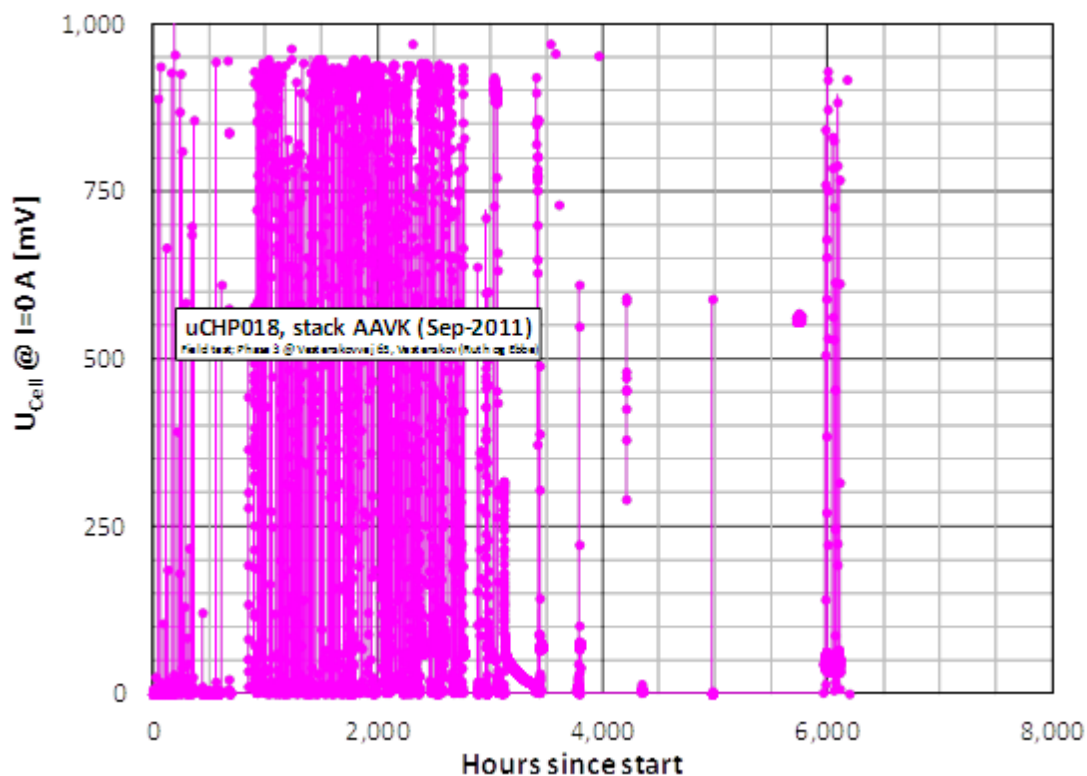
**B (right): Typical pin-holes developed in MEAs tested in a  $\mu$ CHP-unit with the improved hydrogen control system ( $\mu$ CHP020). The shown MEA is based on Nafion 212.**

The field units have been operated differently. The unit without an air check valve (unit  $\mu$ CHP018, Figure 4) has been operated more or less on a continuous basis, while the unit equipped with an air check valve (unit  $\mu$ CHP013, Figure 7), and has been operated on a scheme with 5 hours of operation and 1 hour in idle-mode. The numbers of start/stops are listed on the respective figures. No effects of the start/stop cycle transients have been observed, not taking the resulting OCV exposure into consideration.

The improved MEAs based on Nafion XL100 membrane have proven more than three times increase in lifetime (unit  $\mu$ CHP018, Figure 4). However, the MEAs show a high degradation rate due to  $>800$  mV in idle-mode on windy days in contrast to the unit equipped with an air-check valve. Furthermore, the air-check valve (unit  $\mu$ CHP013, Figure 7) has allowed a slow continuous MEA degradation, as illustrated with the MEA degradation from BoL-performance shown in Figure 8.



A.



B.

Figure 4. Results of the field test with unit  $\mu$ CHP018; A) average cell voltage and produced stack power. Nominal load is  $0.32_{\pm 1}$  A/cm<sup>2</sup>; B) Cell voltages during idle-mode conditions.

A plot of the stack current vs. time is shown in Figure 5.

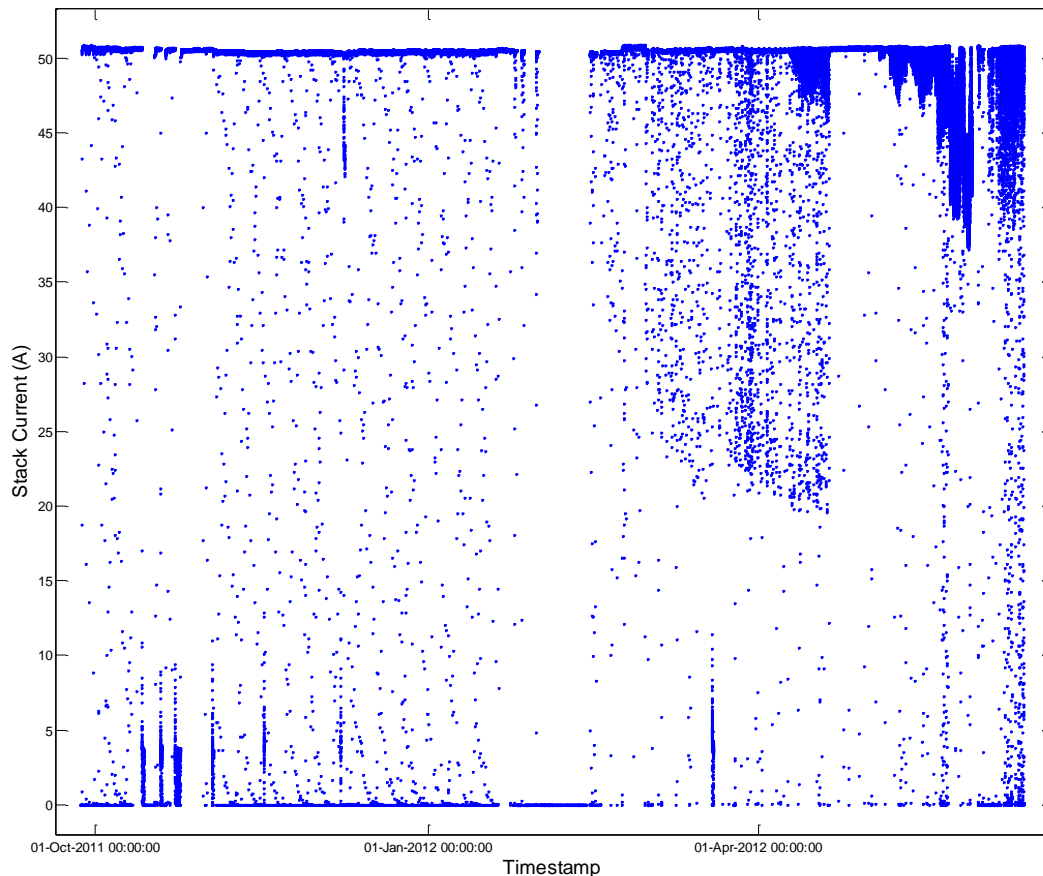


**Figure 5. Stack Current [A] for unit  $\mu$ CHP018 as function of time, showing that the set-point of 50 A could not be maintained towards the end of the test due to degradation. White spot in middle reflect 2 weeks' stop due to freezing water in the  $H_2$  exhaust.**

The profile (Figure 5) shows the ON/OFF nature of the  $\mu$ CHP system controlled by heat demand. The intermittent current levels are caused by the ramp-up to maximum load. The latter part of the experiment shows a change in load profile as more points deviate from maximum current (50A). This is caused by single cells with lower performance. The system tries to recover the performance of these cells by lowering the current while improving the operational parameters for the cells.

A more detailed illustration of the cell voltage for  $\mu$ CHP018 is shown in Figure 6. It is clearly seen that the performance degradation contains considerable recoverable voltage (reversible voltage loss). It also shows that a calculated average degradation rate fails to show the progress of the degradation throughout the experiment. The degradation rate after the two-week stop (due to  $H_2$  exhaust freeze) is higher than before the stop, indicating that detrimental conditions have been encountered.

A conclusion to be drawn from these results shown in Figure 6 is that it is very important to distinguish between reversible and irreversible cell voltage decay. There is clearly some voltage decay which is recoverable, typically due to flooding or dehydration, and this should not be mixed with the irreversible degradation, although these conditions may lead to irreversible degradation.

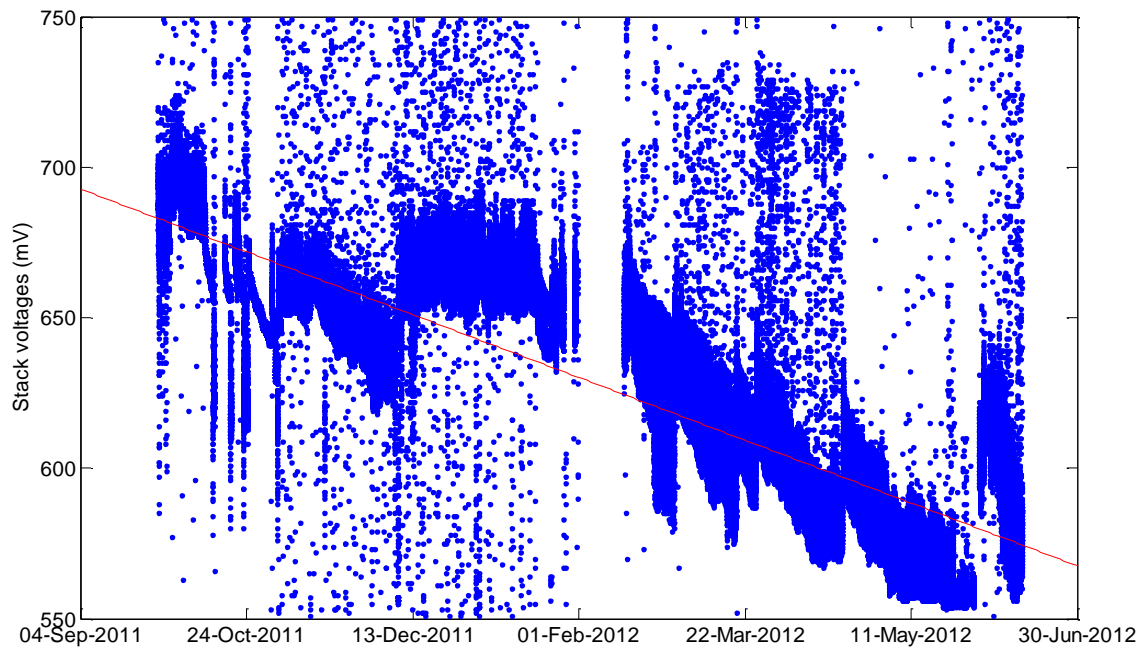


**Figure 6. Cell voltage for unit  $\mu$ CHP018 between 550 and 750 mV, clearly showing degradation. The red line indicates the average degradation of  $\sim 16 \mu\text{V/h}$  over  $\sim 9$  months' operation.**

In the case of  $\mu$ CHP013, more uniformly voltage decay is observed throughout the test (Figure 7). The stack current profile shows no sign of cell degradation as the case is for  $\mu$ CHP018 in Figure 5. The test specific details for  $\mu$ CHP013 are given in Figure 7.

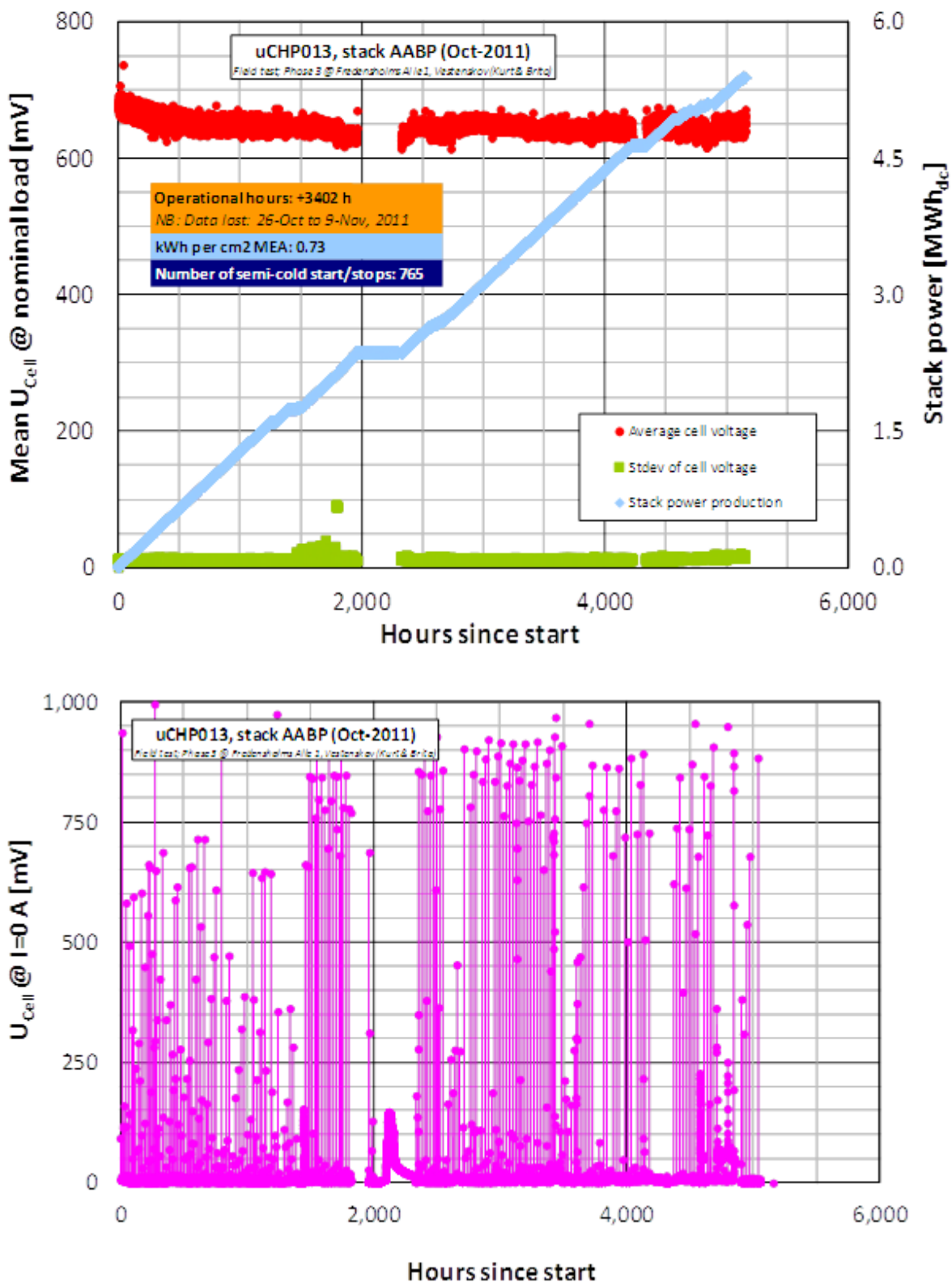


Figure 7. Results of the field test with unit  $\mu$ CHP013; *above*) average cell voltage and accumulated stack output [MWh<sub>DC</sub>]. Nominal load is  $0.32_{\pm 1}$  A/cm<sup>2</sup>; *below*) Cell voltages during idle-mode conditions.

The calculated accumulated degradation rate for  $\mu$ CHP013 is shown in Figure 8.

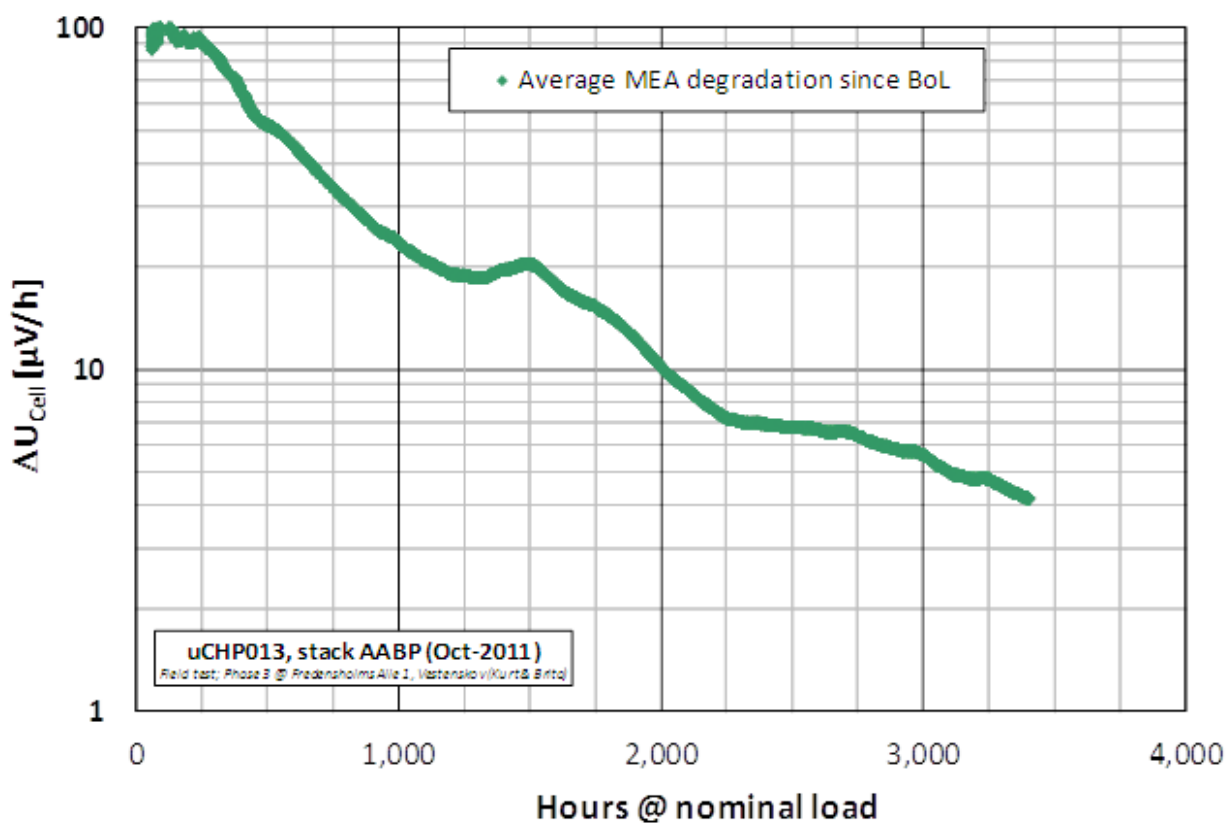


Figure 8 Calculated cell voltage degradation rate [ $\mu\text{V}/\text{h}$ ] for unit  $\mu\text{CHP013}$ , falling from  $\sim 100$  to  $\sim 4$   $\mu\text{V}/\text{h}$ .

The accumulated degradation rate decays roughly logarithmically from about  $100$  to  $4$   $\mu\text{V h}^{-1}$ .

A summary of the test data for comparison of the degradation of stacks  $\mu\text{CHP13}$  and  $\mu\text{CHP018}$  is shown in Table 2.

To evaluate the effect of the installed air-check valve for the cathodes, the difference in OCV exposure between the  $\mu\text{CHP}$  units were investigated. As the data logging frequency for the stacks in idle mode are in the range of  $1\text{-}1.5$   $\log \text{min}^{-1}$ , integration of voltage/time curves is not an option. Instead, a voltage read count for several cut-off voltages was performed. The result is shown in Table 2.

Table 2. Voltage excursion count for  $\mu\text{CHP018}$  and  $\mu\text{CHP013}$ .

Cut-off (mV)	Number of Voltage excursions		Ratio of excursions
	Unit $\mu\text{CHP018}$	Unit $\mu\text{CHP013}$	$[\mu\text{CHP018}/\mu\text{CHP013}]$
1000	10	5	2.0
950	54	56	0.96
900	2505	251	10.0
850	3580	418	8.6
800	4252	555	7.7
750	4802	680	7.1

If assuming cell voltages higher than 800 mV to be harmful, there is considerably higher exposure to these conditions for  $\mu\text{CHP018}$ . The ratio between 8 and 10 is slightly higher than the 6x higher overall degradation rate calculated for  $\mu\text{CHP018}$  (Table 1). The distribution of these counts along the course of the experiment is shown in Figure 9.

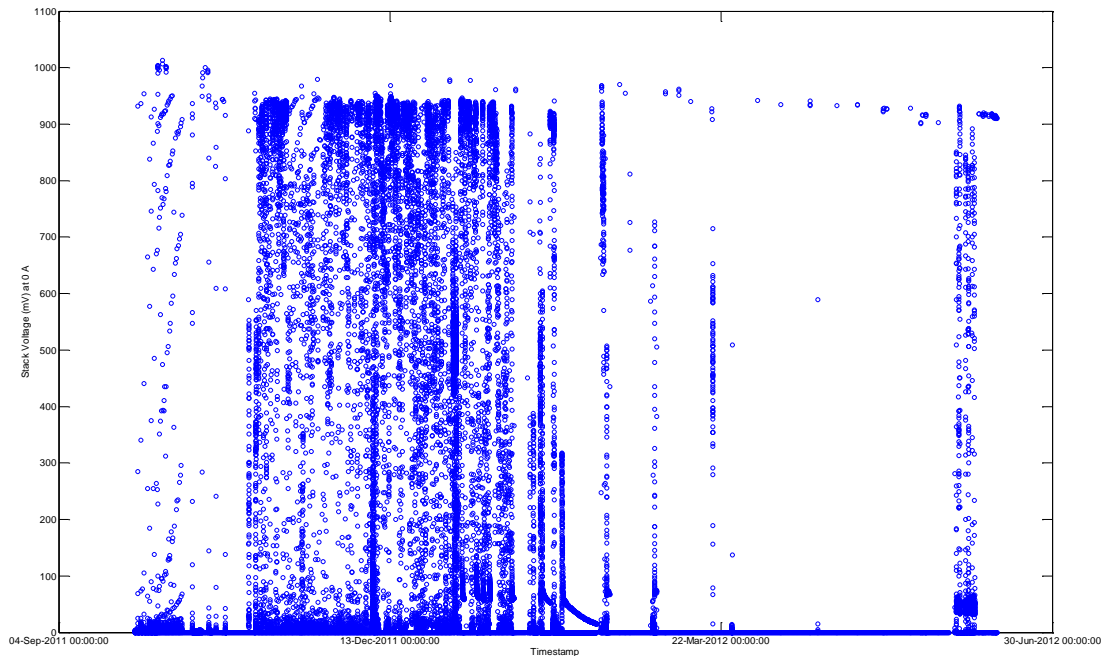


**Figure 9. Distribution of the voltage excursions over the duration of the test for  $\mu\text{CHP018}$  at 0 A.**

For  $\mu\text{CHP013}$ , the voltage excursions are much more uniformly distributed throughout the course of the experiment. It is intriguing to note that the highest voltage excursion counts are found in the time interval where the degradation rate is lowest. Degradation by OCV is known to cause severe, though often uniform, chemical degradation of the membranes. The observed degradation of the system might therefore be offset from the actual degradation taking place, like when the mechanical integrity of the membrane is compromised thus resulting in gas cross over.

## 1.4 Conclusions from real life field tests

The critical operational parameters have proven to be as follows:

- OCV conditions should preferably be avoided or at least limited to a minimum (air check valve or closed air loop in idle conditions).
- Hydrogen control (relative humidity, start-up etc.).

Dry hydrogen fuel accelerate the membrane degradation, membrane failure in the gas-inlet has been one of the main MEA end-of-life courses. The mitigation strategy is to implement an improved hydrogen control system to ensure some hydrogen humidification and improve the start-up situation.

Degradation by OCV conditions is severe and often one or more decades in magnitude higher than the other contributions to the overall degradation rate. It is therefore difficult to assess the effect of these other contributions when the system is significantly exposed to OCV conditions. In the comparison between the stacks  $\mu$ CHP018 and  $\mu$ CHP013, the stacks have almost the same number of start and stops. To discern the effect of start and stop on the system is therefore difficult in the presence of OCV voltage excursions, even if it is well established that the transients in temperature and relative humidity are known to cause degradation.

Moreover, examination of the results (e.g., Figure 6) shows that it is very important to distinguish between reversible and irreversible cell voltage decay. There is clearly some voltage decay which is recoverable, typically due to flooding or dehydration, and this should not be mixed with the irreversible (non-recoverable) degradation when conclusions are drawn. Thus, reversible voltage decay should preferably be "removed" prior to determination of the true irreversible degradation rates.

## 2 Results and experiences from phase 1 of Accelerated Stress Tests

### 2.1 Introduction

In this chapter, the results from the execution of the first phase of the accelerated stress test (AST) program carried out in WP2 (documented in D2.2) are evaluated. Initially, however, the challenges encountered including those related to the use of factorial designed experiments are discussed, revealing the vulnerability of this method when it turned out that we were not able to complete the ASTs and obtain results from the full  $2^3$  factorial experiments.

### 2.2 Challenges encountered in phase 1 of the AST program

#### 2.2.1 Inter-laboratory variance

The application of factorial design experiments<sup>5,6</sup> reduces the number of experiments required to evaluate a given number of experimental variables (factors) under study. A requirement for this reduction is, however, that all experiments are successfully completed. The initial idea for the project was to divide the AST protocols between project partners, to ensure true collaboration between partners. A requirement for this distribution of work is knowledge of the inter laboratory variance. A baseline performance test was therefore conducted. The results of this evaluation were presented by ECN at the 2<sup>nd</sup> progress meeting in January 2011.

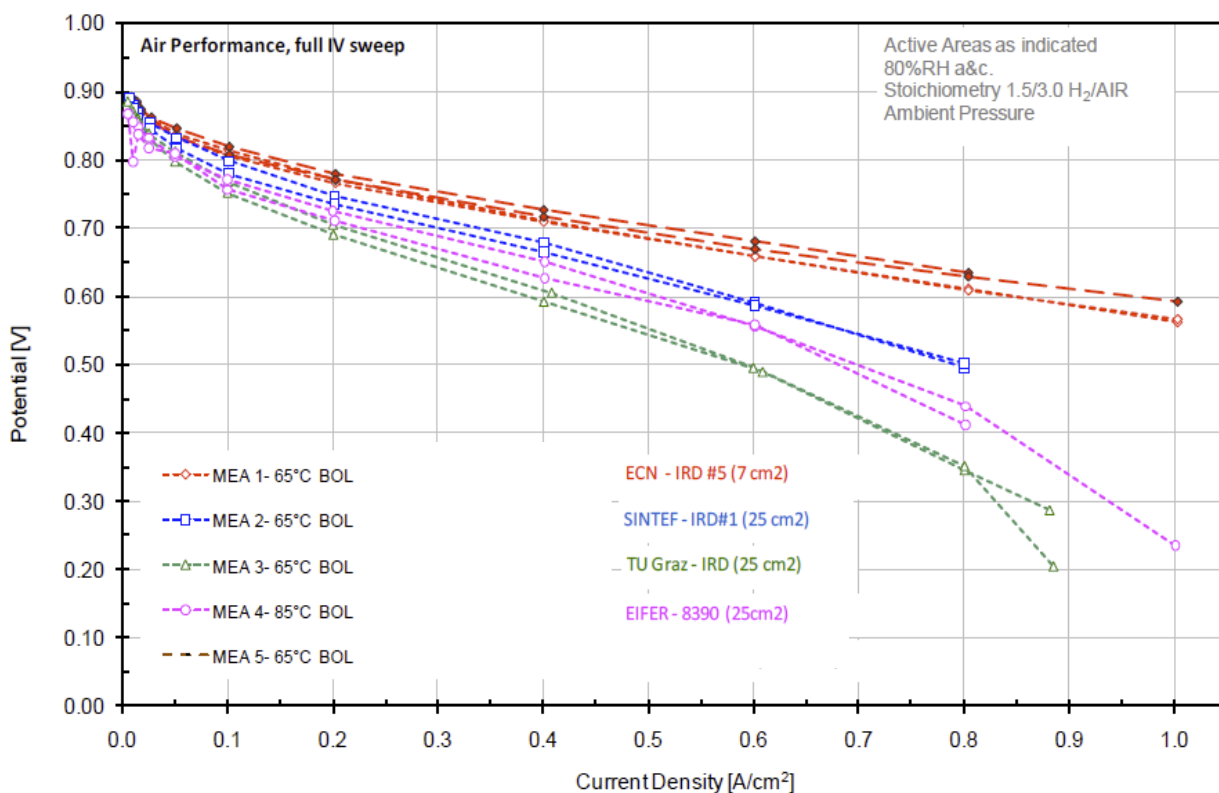


Figure 10. Results from baseline performance test to reveal inter laboratory variance.

<sup>5</sup> G.E.P. Box, W.G. Hunter and J.S. Hunter, "Statistics for experimenters – An Introduction to Design, Data Analysis, and Model Building", Wiley, 1978.

<sup>6</sup> Report D5.1: "Experimental Guideline for Designed Experiments", KEEPEMALIVE project, FCH JU, Grant Agreement Number 245113.

The results from the baseline performance test were very conclusive on the fact that variance was too large to divide the execution of AST protocols between the laboratories. That smaller cells perform better than larger cells is natural and expected. But, for cells of the same 25cm<sup>2</sup> active cell area using similar test fixtures by partners SINTEF, TUG and EIFER, cell performance varied more than 30% at high current densities (Figure 10). One laboratory, thus, had to complete the whole set of experiments for that AST protocol originally planned to be shared with another partner. This unfortunately lead to extra work related to the fact that some initial results could not be used for later evaluation because they did deviated too much from the other results found for the same AST protocol at the other partner's laboratory.

### 2.2.2 Standard deviation and unstable operation

In fuel cell durability research, evidence of repeated or parallel experiments is scarcely found. In statistical evaluation of fuel cell degradation data, it is important to establish knowledge of the variance between experiments for the fuel cell test configuration. In KeePEMalive, the break-in of the fuel cell was performed at identical conditions for all ASTs. As an example, the voltages at the end of the break-in period for six experiments performed by EIFER are shown in Table 3.

**Table 3. Averaged cell voltage data for the last 200 minutes of the cell break-in period for five experiments conducted by EIFER for the Continuous operation AST at 400mA cm<sup>-2</sup>.**

Test ID	Mean Cell voltage (V)	STDEV (mV)
8414	0.5633	5.4
8390	0.6357	2.6
8434	0.6266	1.9
8458	0.5985	1.4
8346	0.6686	2.3
<b>Average (V)</b>	<b>0.6185</b>	
<b>STDEV (V)</b>	<b>0.0397</b>	
<b>RSD (%)</b>	<b>6.4</b>	

The relative standard deviation (RSD) of the cell voltage at 400 mA cm<sup>-2</sup> is 6.4 %. Although this RSD should be calculated for the relevant current density levels to be evaluated, it gives good indication of the magnitude of a change in voltage, as a response to a change in operational set point(s), required for an effect to be considered significant. The RSD observed for these experiments were considered to be satisfactory with respect to the responses expected from these experiments.

For the initial set of AST protocols as described in D 1.2, all eight protocols were set up with a 2<sup>3</sup> design. None of these AST experimental protocols were completed with the full set of eight experiments. The main reason for this failure can be traced back to the experimental set point values defined in D 1.2. These values were chosen as a best guess targeting at a representative degradation over the 400 hour test duration. During execution of the AST experiments, it has been found that some of these experimental conditions:

1. Does not allow for stable cell operation (examples and more details may be found in D2.2)
2. Causes very high degradation rates incompatible with characterization frequency

### 2.2.3 Break-in procedure not adequate for new, improved membrane materials

The initial break-in procedure prescribed for the initial AST protocols was shown to be insufficient for providing optimal performance at the start of the experiment. While evaluating the data from the Continuous Operation AST protocol (section 2.3.1), it was found that the fuel cell break-in procedure was insufficient for the new generation membranes. From the UI curves of several tests it was found that the performance after 200 hours was better than that at the beginning of test. This makes evaluation of the results difficult as the performance gain must be known to correct the degradation rate. The polarization curves of Test 8414 are shown in Figure 11 to illustrate this point.

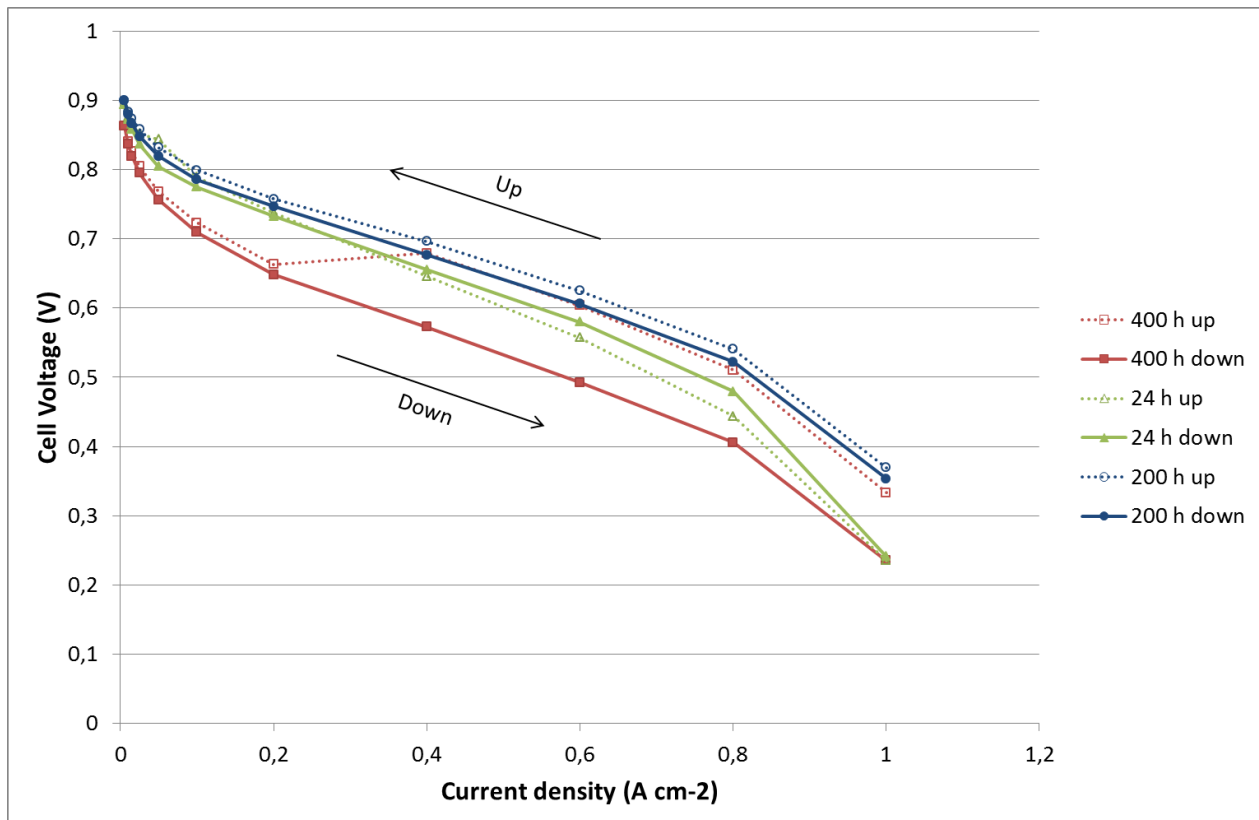


**Figure 11.** Performance characterization for experiment 8414 of the Continuous Operation AST at after break-in (24h), at 200h and 400 h operation, showing that the initial break-in procedure is not adequate for the new membranes under study.

### 2.2.4 Implications for the interpretation of AST results

High inter-laboratory variance, instable operation at several of the selected sets of operation conditions, and insufficient break-in procedure as new improved membrane materials were introduced, lead to severe problems of interpreting the results from phase one of the AST program. These challenges call for a complete restructuring of the AST program in phase 2, as described in Chapter 4.

## 2.3 Findings from individual AST protocols

Three key problems were encountered when carrying out phase 1 of the AST program as described in the section 2.2:

1. High inter-laboratory variance, and
2. Levels of factors (e.g., T, RH, Current Density) selected outside the stable operation region
3. Insufficient break-in procedure as new improved membrane materials were introduced

In this section we have interpreted the results statistically from two AST protocols from which the result from phase 1 are considered adequate and reliable. Those protocols for which statistical analyses are not possible, are briefly commented on in section 2.3.3.

### 2.3.1 Interpretation of results from Continuous Operation AST protocol

The continuous operation protocol was intended in D1.2<sup>7</sup> to be a reference to the other AST protocols where one or more means to exacerbate degradation are applied. It turned out that completing eight experiments for a full 2<sup>3</sup> factorial design was impossible for the set points of the operation variables selected (T, RH and Current Density), see section 2.2.2. The four experiments which were successfully executed for the Continuous Operation AST protocol are listed in Table 4.

**Table 4. Experiments successfully executed under the Continuous Operation AST protocol, including high (+) and low (-) levels and duration of experiment.**

EXP #	T (°C)	RH (%)	Current Density (J) (A cm <sup>-2</sup> )	Duration (hours)
8434	65 (-)	80 (+)	0.6 (+)	400
8414	65 (-)	40 (-)	0.2 (-)	400
8458	85 (+)	40 (-)	0.6 (+)	225
8390	85 (+)	80 (+)	0.2 (-)	338

An estimate of the degradation rates was obtained for the 4 cells which were successfully executed. These estimates were used to calculate the main degradation effect of the three factors given in Table 6.

**Table 5. Calculation of main degradation effects [mV h<sup>-1</sup>] for the Continuous Operation AST protocol.**

Factor (unit)	Confounded with Interaction	Average degradation rate [mV/h]		Main Effect of Factor
		High level	Low level	
T (°C)	RH x J	-1.5	-0.3	-1.2
RH (%)	T x J	-0.5	-1.3	0.8
J (Acm <sup>-2</sup> )	T x RH	-1.6	-0.2	-1.4
Average				-0.9

<sup>7</sup> D1.2 Initial set of AST protocols.

These main effects are found by calculating the contrast between degradation rates at high and low level of each factor under study<sup>8</sup>.

As expected, degradation rates are lower at high RH, giving a positive Main Effect for this factor. More surprisingly, the main effects of Temperature and Current Density (J) are comparable in magnitude. This may be explained by a contribution from the TxRH interaction which is confounded with the factor Current Density for this set of data (see Table 5). Completion of all eight AST experiments of the 2<sup>3</sup> design is required in order to resolve the effect of J from TxRH.

The calculated effects should be considered with some scrutiny: The estimate contains reversible as well as irreversible degradation contributions. In addition, there is a performance gain that is of unknown magnitude that might affect the degradation rate estimates obtained, linked to the insufficient break-in procedure applied (as described in section 2.2.3).

### 2.3.2 Interpretation of results from Fuel Starvation AST protocol

Fuel starvation is known to degrade the fuel cell anode by causing elevated anode potentials. Insufficient hydrogen supply may lead to negative cell voltage when the cell is operated in constant current mode. For the Fuel Starvation experiments carried out in the KeePEMalive project, partner TUG chose to vary current density, while keeping hydrogen supply constant, giving stoichiometries of 1,5 and 0,9 respectively. During under-stoichiometric conditions, the cell starves and cell voltage reaches negative values. The cell voltage for an experiment performed under the AST fuel starvation protocol is shown in Figure 12.

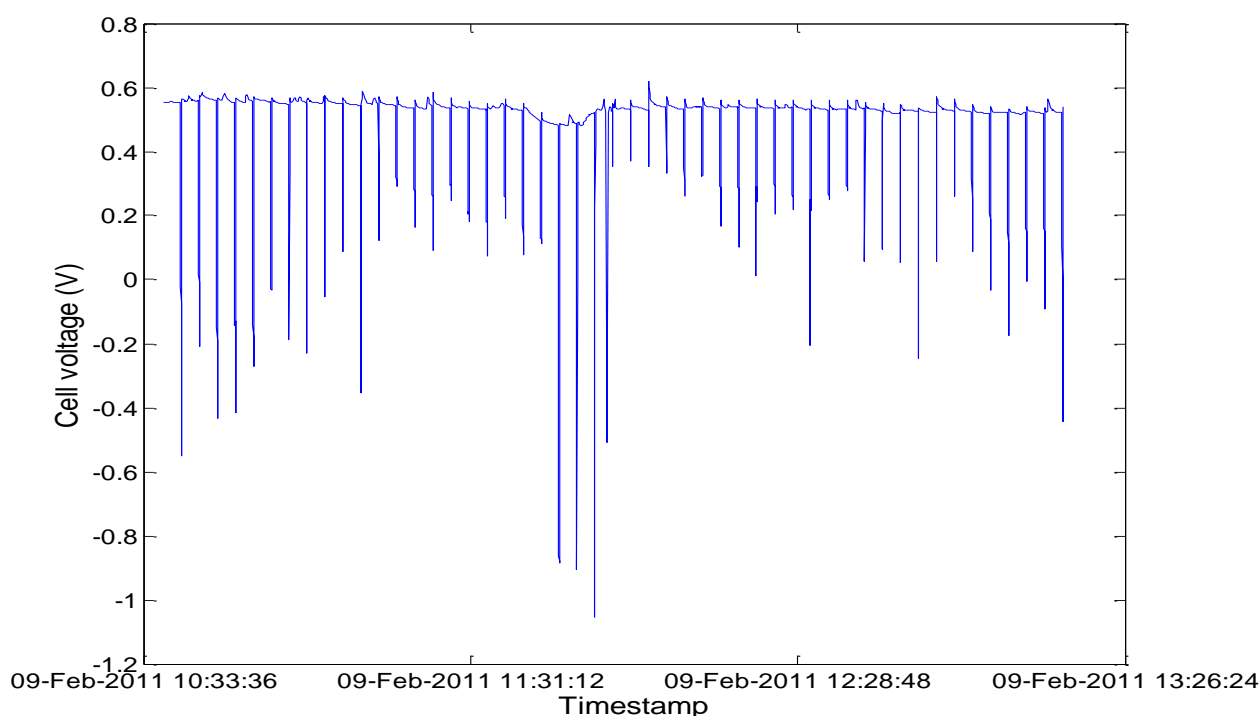


**Figure 12. Cell voltage for the 50 first cycles of test EXP1 for the Fuel Starvation AST protocol (see Table 6).**

---

<sup>8</sup> These calculations are explained in D5.1 “Experimental Guideline for Designed Experiments”, KEEPEMALIVE project, FCH JU, Grant Agreement Number 245113.

The six experiments performed for the Fuel Starvation AST protocol comprises a fractional factorial  $2^{3-1}$  design of experiments with experiments 5 and 6 as replicates of experiments 3 and 4, the latter two executed using a segmented cell hardware.

The End of Test (EoT) criterion for termination of these experiments was the hydrogen cross-over current exceeding  $5 \text{ mA cm}^{-2}$ . A comparison between the time dependence of the cross-over current for two cells is shown in Figure 13.

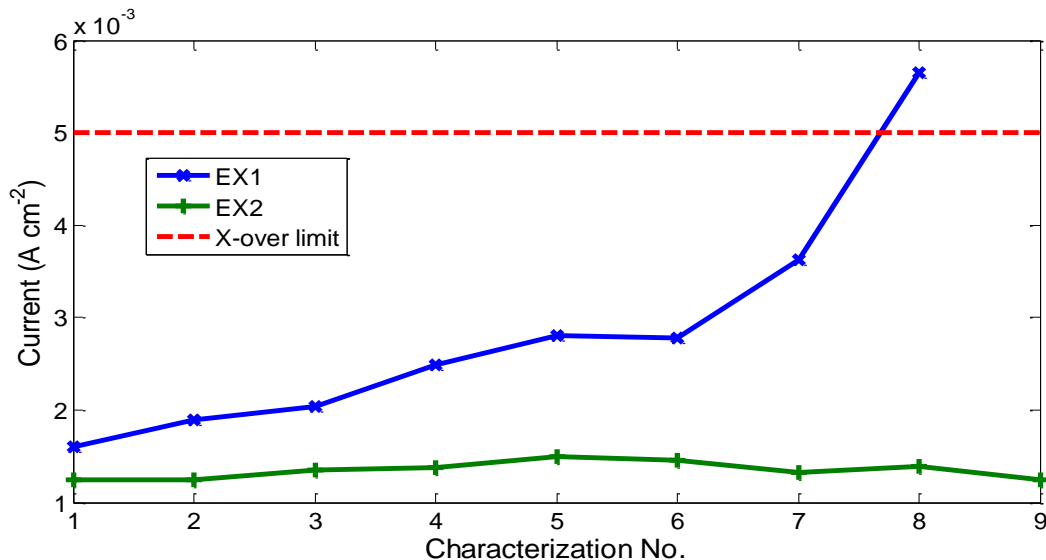


Figure 13. Hydrogen cross-over current density for EXP1 and EXP2, including the EoT-limit of  $5 \text{ mA cm}^{-2}$ .

For the cell from EXP1 the typical exponential relationship is seen towards the end of the test. EXP2 never failed the EoT criterion of  $5 \text{ mA cm}^{-2}$ . The cells were exposed to approximately ten starvation cycles per hour. It is interesting to find that for EXP2, hardly any cross-over current was developed over almost 500 hours of testing. This is intriguing and we cannot identify any evident relationship between this response and the other responses evaluated for this AST protocol.

The hydrogen gas cross-over rate was evaluated by potentiostatic monitoring of current at 0.43 V. The initial cross-over rate for all experiments is shown in Figure 14.

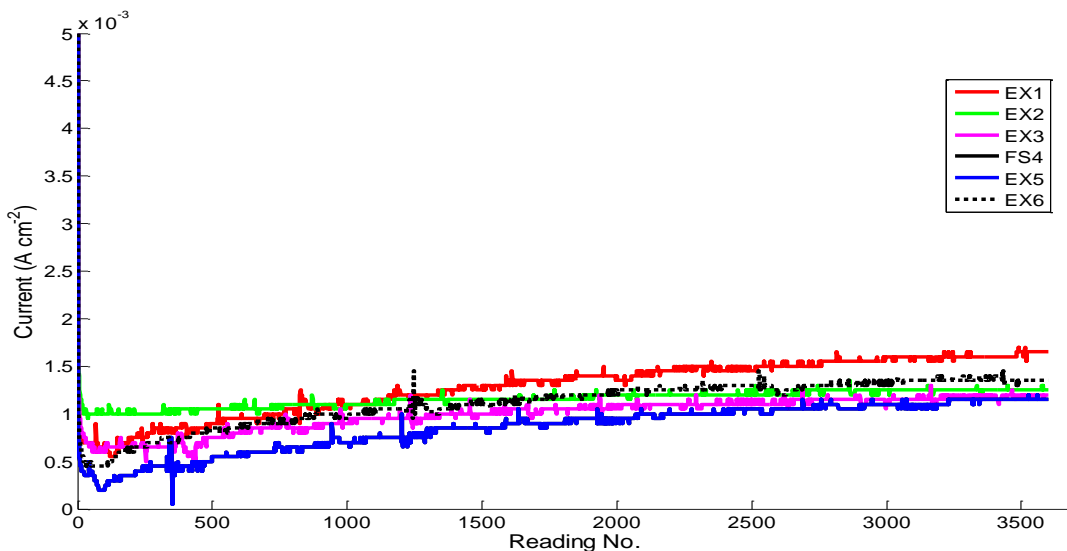


Figure 14. Initial hydrogen gas cross-over current densities.

Calculated from an average of the readings 3000 to 3500, the average cross-over current was found to be  $1.3 \text{ mA cm}^{-2}$ . The relative standard deviation of the average was 14.5 %, suggesting higher variance than the case for those obtained of ECSA and EIS. The source of variance might found in the analytical technique although the analytical error for both ECSA and cross-over assessment should be fairly identical; both employing the same potentiostat and connections.

Whereas replicate experiments 4 and 6 had the same duration (200 starvation cycles before hydrogen gas cross-over current exceeded  $5 \text{ mA cm}^{-2}$ ), replicate experiments 3 and 5 did vary significantly: 400 and 50 starvation cycles respectively. Despite the significant discrepancy in durability, the mean value of these experiments was used for further statistical evaluation of the results. The experimental conditions for the individual experiments are given in Table 6.

**Table 6. Experiments successfully executed under the Fuel Starvation AST protocol, including high (+) and low (-) levels and Number of starvation Cycles of the experiments.**

EXP	T (°C)	RH (%)	J (A cm <sup>-2</sup> )	No. Cycles
1	65 (-)	40 (-)	0.2 (-)	1700
2	65 (-)	80 (+)	0.4 (+)	1750
3/5	85 (+)	40 (-)	0.4 (+)	225
4/6	85 (+)	80 (+)	0.2 (-)	200

A  $2^{3-1}$  fractional factorial experiment allows for calculation of the main effect of each of the three factors, given the assumption that the main effect of each factors is larger than the interaction between the remainder two factors. The result of the calculation is shown in Table 7.

**Table 7. Calculation of main effects from the number of cycles performed. All effects are in number of cycles.**

Factor (unit)	Confounded with Interaction	Average No Cycles		Main Effect No. of Cycles
		High level	Low level	
T	RH x J	213	1725	-1512
RH	T x J	975	963	12
J	T x RH	988	950	38
Average				969

The results found in Table 7 are hardly surprising. It can be directly deduces from Table 6 that temperature has a huge impact on the test duration. The calculations also show that the other two main effects are not significant. It should be mentioned, though, that using the average of 50 and 400 starvation cycles for the two replicate cells (No. 3 and 5) may be criticized and should be further discussed.

The result found in Table 7 only correlates to how the fuel cell degradation is estimated. In this case, the number of fuel starvation cycles is evaluated against the End-of-Test (EoT) criterion of hydrogen cross over current. It does not directly reflect the performance degradation of the fuel cell,

beyond that of the inflection of hydrogen cross-over on fuel cell performance. Therefore, another approach was taken to evaluate explicitly the effect of the factors on degradation based on the available performance data.

Based on the performance data current densities were selected to assess whether degradation varies between the typical regions of the polarization curve:

- a) Activation region ( $\sim 0-100 \text{ mA cm}^{-2}$ )
- b) Linear (ohmic) region ( $\sim 100-500 \text{ mA cm}^{-2}$ )
- c) Mass transfer diffusion limitation region ( $\sim > 500 \text{ mA cm}^{-2}$ )

The performance decay was calculated by performing a linear regression through all polarization curves for all six cells throughout the duration of the respective ASTs. To simplify the task, all cell voltage data at each current density level were averaged (i.e., both scan directions). This was done for all current densities except for 800 and 1000  $\text{mA cm}^{-2}$ , where data typically were missing from the later part of the AST experiments due to degradation. As an example, polarization curves for Experiment 2 (EXP2) throughout the duration of the AST experiment are shown in Figure 15. As can be seen the performance clearly deteriorates over time, but again the problem of the insufficient break-in for the new improved membranes is revealed (as discussed in section 2.2.3).

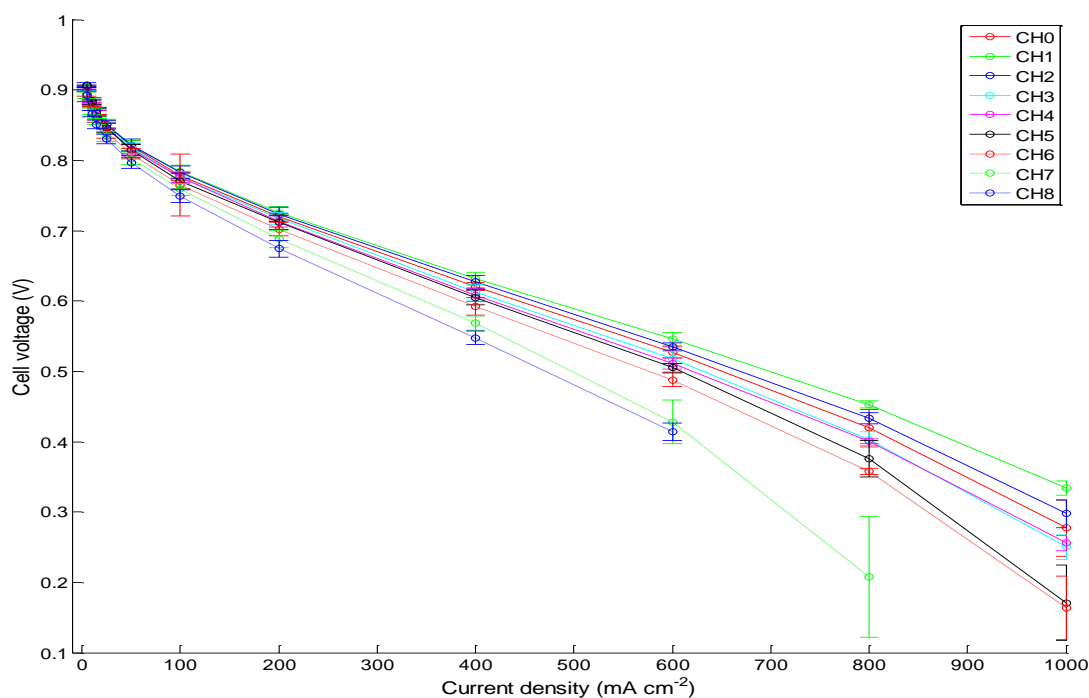


**Figure 15. Polarization curves for fuel starvation experiment no.2 (EXP2) showing that performance is increasing from the start (after break-in, 24 hours CH0) and reaches a "peak" at the second reading (CH1 at 72 hours) before it shows falling performance caused by the starvation cycles which this cell is exposed to.**

The corresponding degradation rate regressions for all six cells are shown in Figure 16.

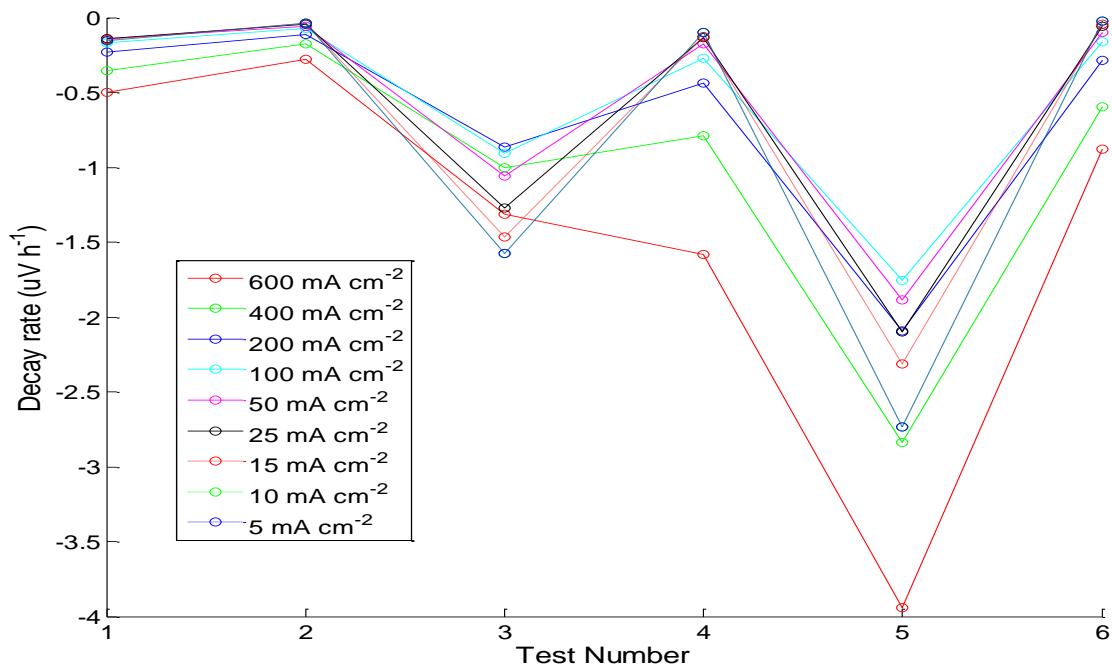


**Figure 16. Estimated degradation rates for the six experiments of the Fuel Starvation AST protocol. For experimental conditions, please refer to Table 6.**

The interpretation of the results is easier starting from the average degradation rate of each test. This average and its corresponding standard deviation are illustrated in Figure 17.

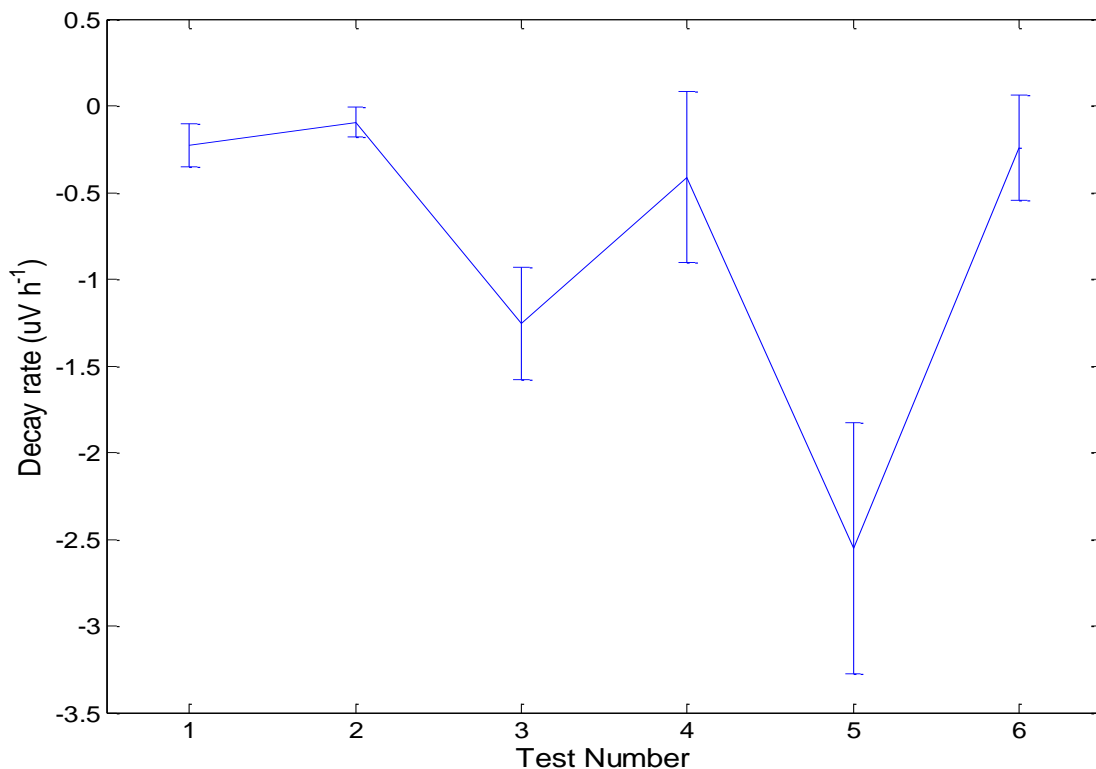


**Figure 17. Averaged degradation rates for the six fuel starvation experiments with standard deviation. Test number 4 and 6 are replicates of tests 3 and 5, respectively, using a segmented cell.**

Clearly, the averaged degradation rates correlate with the number of fuel starvation cycles; whereas EXP2 at 1750 cycles has the lowest degradation rate average, EXP5 at 50 cycles clearly has the highest degradation rate. EXP3 has a lower average degradation rate that would be expected from the 400 cycle duration. Again, the discrepancy between replicate experiments EXP 3 and EXP 5 can be seen (standard deviations not overlapping), clearly indicating that one of these should preferably be disregarded in the data interpretation. It may be speculated whether the use of the segmented cell fixture for EXP5 may have introduced some unexpected features which are not understood. A much higher internal resistance for EXP5 compared to EXP3 (Table 12) may be linked to this finding, but cannot be taken as the full explanation.

Another interesting feature of Figure 17 is the standard error bars. From fuel cell durability one would expect the standard deviation to increase as the performance penalty tends to be more severe at higher current densities. Returning to Figure 16, the cause of the increased standard deviations can be correlated to the increased degradation rates at higher current densities. For EXP4 and EXP6 it can be seen that the estimated degradation rates at low current densities are much lower than those of EXP3 and EXP5. As all of these experiments were performed at 85 °C, this suggests that either relative humidity or current density contributes to the degradation rate at low current density.

In order to explore these observations further, main effects were calculated for both averaged (Figure 17) and individual degradation rates for degradation rates at various current densities between 50 and 600 mA cm<sup>-2</sup> (Figure 16). The degradation rates used to calculate main effects are shown in Table 8.

**Table 8. Calculated degradation rates at selected current densities. Avg. indicates the average degradation rate for all tests.**

EXP	Factors and levels			Degradation Rate (mV h <sup>-1</sup> )			
	T	RH	J	@ Current density [mA cm <sup>-2</sup> ]			Mean
	(°C)	(%)	(A cm <sup>-2</sup> )	50	400	600	
1	65	40	0.2	-0.14	-0.36	-0.50	-0.22
2	65	80	0.4	-0.06	-0.18	-0.28	-0.09
3/5	85	40	0.4	-1.47	-1.92	-2.63	-1.90
4/6	85	80	0.2	-0.14	-0.69	-1.23	-0.33
<b>Avg.</b>				-0.45	-0.79	-1.16	-0.63

In general it can be concluded that the degradation rates are higher at higher current densities for a given cell. This indicates that diffusion (mass transfer) limitations are experienced and limiting the performance at high current densities. This may be linked to changes in the gas diffusion layers (GDLs) and should be explicitly examined in the further work in WP3.

From these degradation rates, the main effect of each factor was calculated as the difference between the average degradation rate at high and low levels of the factor, respectively. The calculated main effects are shown in Table 9.

**Table 9. Calculated Degradation Rates of Factors for the Fuel Starvation AST experiments.**

Factor (Unit)	Confounded w/Interaction	Degradation Rate (mV h <sup>-1</sup> )			
		@ Current Density [mA cm <sup>-2</sup> ]			
		50	400	600	Mean
T (°C)	RH x J	-0.70	-1.04	-1.54	-0.96
RH (%)	T x J	0.71	0.70	0.81	0.85
J (A cm <sup>-2</sup> )	T x RH	-0.62	-0.52	-0.59	-0.72

From the main effect calculated from the mean of the selected current density of the polarization curve, the average effect is  $-0.63 \text{ mV h}^{-1}$  (Table 8) The effect of temperature was found to be  $-0.96$  and current density  $-0.72 \text{ mV h}^{-1}$  (Table 9). This means that both high temperature and high current density increases the degradation rate of the fuel cell. On the other hand, relative humidity has opposite sign; higher RH lowers the degradation rate. The effects are comparable and similar in magnitude to the average effect.

Evaluating the main effects calculated from the selected Current Density reveal one interesting aspect: whereas the effects of Relative Humidity and Current Density appear to be fairly constant over the polarization curve, this is not the case for temperature. From current densities ranging from 50 to 600 mA cm<sup>-2</sup>, the effect of temperature on the degradation rate is more than doubled. This may indicate that Temperature is the main factor inducing material changes in the morphology (hydrophobicity/hydrophilicity) of the Gas Diffusion Layer or linked to the loss of carbon from the catalyst layer as discussed later in this section.

From the calculations of the main effects of individual current densities, it can be seen that the effect of temperature is more dominating than the other effects at higher current densities. There are several possible mechanisms that could explain the degradation, among them catalyst degradation and degradation of gas diffusion layers limiting the transport of reactants and reaction products to and from the electrodes.

Setting aside statistical evaluation of the result shown in Figure 17, a slightly different conclusion might emerge when looking at the data. For experiments 3/5 and 4/6 it is evident that another effect than Temperature (85 °C for all) is responsible for the higher degradation rate for experiments 3/5. It is well documented that low Relative Humidity has a detrimental effect on fuel cell durability, and it would be tempting to assign the difference to an effect caused by the low Relative Humidity. This may then indicate that the effect of the Current Density to be negligible.

The execution of the Fuel Starvation protocol was also conducted with intermittent electrochemical characterization. Cyclic Voltammograms (CV) were used to calculate the initial subsequent loss of ElectroChemical Surface Area (ECSA) of the cathode. The area under hydrogen discharge part of the curve was found by integration of the middle cyclic voltammogram. The contribution from the double layer charging was subtracted by linear regression from the region between 0.4 and 0.5 V.

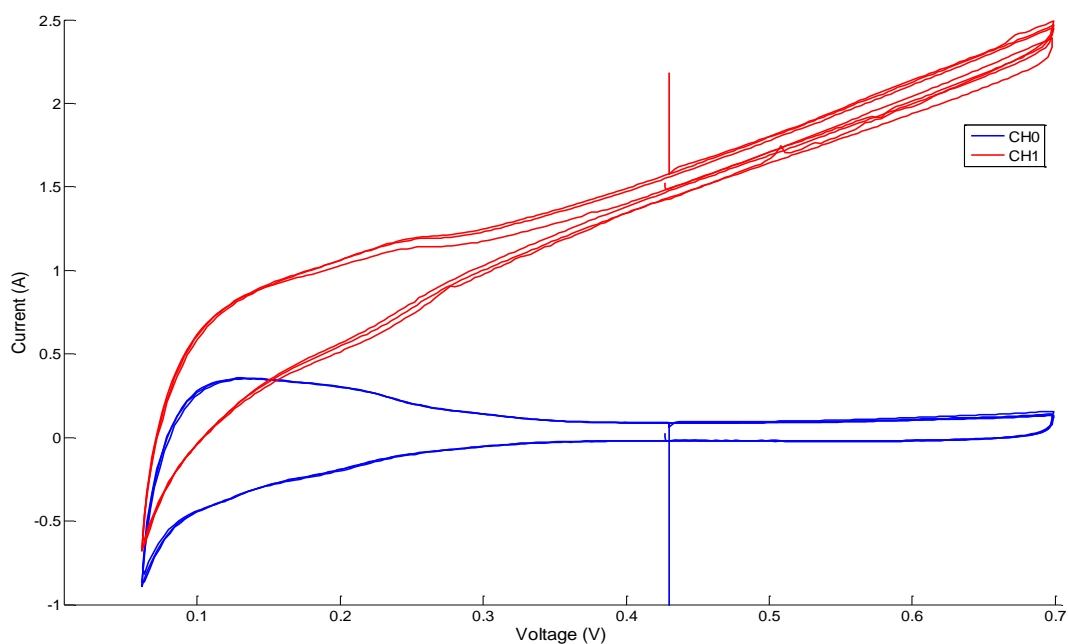


**Figure 18. Cyclic Voltammogram for EXP3 at Beginning of Test (BoT) (CH0) and after 72 hours (CH1).**

For the fast degrading experiments, EXP3 and EXP5 short-circuit was evident from an increase in the CV slope. This is shown for EX3 in Figure 18.

For EXP5 it was found that the ECSA was higher after 24 hours than at Beginning of Test (BoT). With the high degradation rate observed, it is more likely that the curve integration for a CV with higher slope introduces error. The estimates of the loss of ECSA are therefore marked with red for EXP3 and EXP5 in Table 10.

**Table 10. ElectroChemical Surface Area (ECSA) data for Fuel Starvation protocol. Slope and Yint are the linear regression parameters. Calculated estimated ECSA loss extrapolated to 400 hours are also included.**

	Initial ECSA		Linear regression		Est. Loss (m <sup>2</sup> /g) 400h
	mC	m <sup>2</sup> /g	Slope	Yint	
<b>EX1</b>	704.0	26.82	-0.016	30.35	2.91
<b>EX2</b>	867.3	33.04	-0.070	34.48	26.64
<b>EX3</b>	806.4	30.72	-0.038	30.72	15.00
<b>EX4</b>	909.5	34.65	-0.047	34.17	19.11
<b>EX5</b>	734.9	28.00	0.196	28.00	-78.48
<b>EX6</b>	752.0	28.65	-0.043	30.10	15.63
<b>mean</b>	795.7	30.31			
<b>SD</b>		3.06			
<b>RSD</b>		10.1			

ECSA was calculated from the charge found from the area under the hydrogen dissociation part of the curve, a cathode loading of  $0.5 \text{ mg Pt cm}^{-2}$  as well as a specific capacity of  $0.21 \text{ mC cm}^{-2}$ .

The variance in ECSA for all six tests was found to be 10 %. Evidence of insufficient break-in of the cell (lack of catalyst activation) was again observed for several of the tests (see section 2.2.3). The relative variation of 10% might be reduced if MEAs had been properly broken in.

As an example, the calculated ECSAs for EX1 are shown in Figure 19.

In order to evaluate the losses in ECSA, an extrapolation to 400 hours was done. With the exclusion of EXP3 and EXP5, the average loss of ECSA over 400 hours is about 50%. But with the exclusion of EXP3 and EXP5, statistical evaluation is not possible. By looking at the data in Table 10, the large difference in ECSA loss between EXP1 and EXP2 might be explained by higher loss of Pt by dissolution in a larger volume of water originating from RH and possibly also operation at higher current density (more water production).

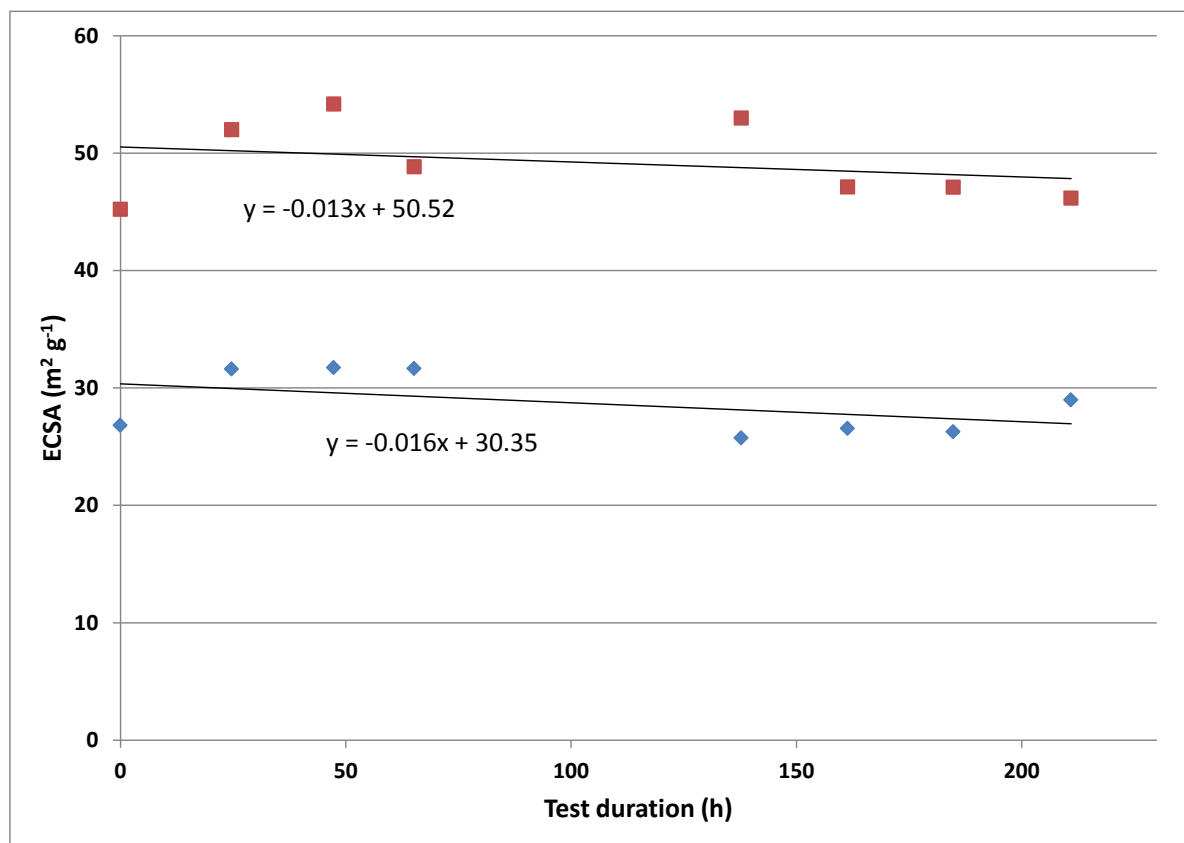


**Figure 19.** Calculated ECSA for EXP1 of the Fuel Starvation protocol. Red dots are from hydrogen adsorption, blue from desorption. Insufficient break-in is indicated by the increasing ECSA with time (section 2.2.3).

For all six experiments, gas analysis was performed for  $\text{CO}_2$  in the anode exhaust. The results are not easily shown superimposed, thus a timeline illustration is shown in Figure 20.

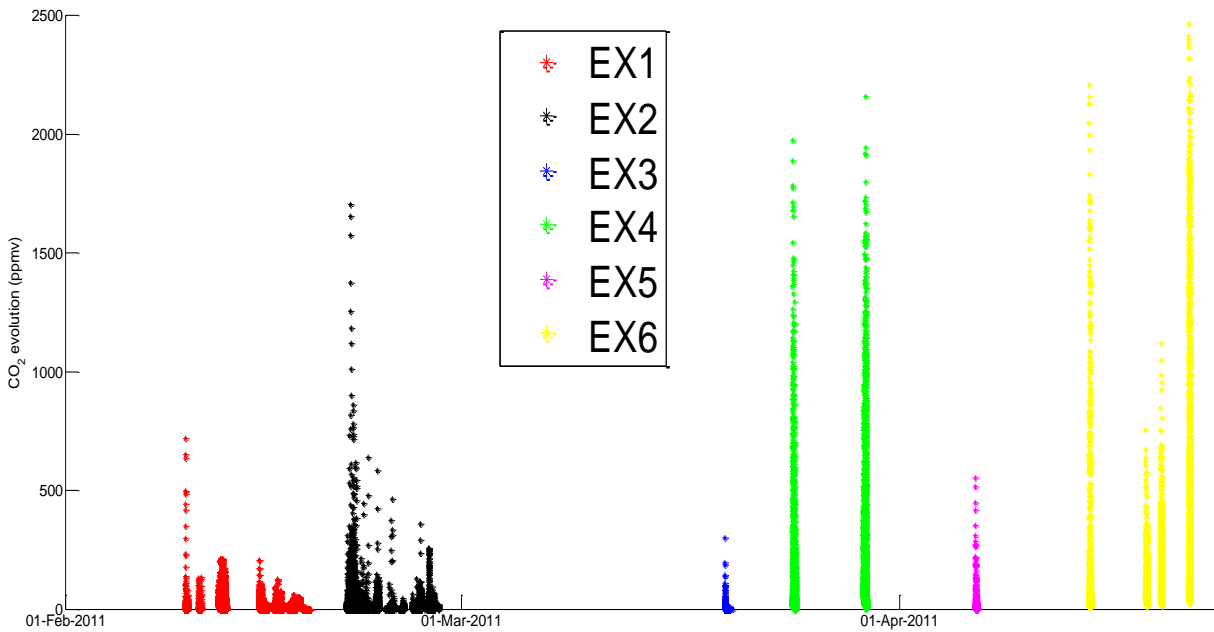


**Figure 20. Carbon dioxide (CO<sub>2</sub>) gas analysis data [ppm] from the anode for six experiments (EXP1-EXP6) of the Fuel Starvation ASTs. Six gas samples were measured for EXP1 but only one for EXP3.**

The main features are summarized in Table 11.

**Table 11. Gas analysis data from the anode for six experiments (EXP1-EXP6) of the Fuel Starvation ASTs.**

	Samples	Max CO <sub>2</sub> (ppm)	Max CO <sub>2</sub> produced (in sample)
<b>EXP1</b>	6	720	3
<b>EXP2</b>	7	1704	1
<b>EXP3</b>	1	300	1
<b>EXP4</b>	2	2160	2
<b>EXP5</b>	1	552	1
<b>EXP6</b>	4	2464	4

The most striking feature of the data is that the high degradation rate of tests EXP3 and EXP5 are not reflected in their CO<sub>2</sub> emissions. These parallel experiments show the same trend in gas evolution: decaying with time. Also, for the other set of replicate experiments, EXP4 and EXP6, the gas analysis is coherent: both show high and sustained CO<sub>2</sub> emission.

The CO<sub>2</sub> emissions from gas analysis at the anode naturally does not correlate well with the ECSA estimates obtained in Table 10, as the latter are characterization of the cathode.

Electrochemical Impedance Spectroscopy (EIS) was performed at Beginning of Test (BoT) and End of Test (EoT) for all tests. EIS spectra were recorded at 50, 100 and 200 mA cm<sup>-2</sup>. Two repeated measurements were performed. The relative standard deviation for the cell resistance at BoT was found to be 20, 12 and 8.8 mOhm for 50, 100 and 200 mA cm<sup>-2</sup>, respectively. Also, the variance between parallels was lower. The 200 mA cm<sup>-2</sup> data is presented in Table 12.

**Table 12. EIS data (at 200 mA cm<sup>-2</sup>) for the six cells of the Fuel Starvation ASTs. \*Experiments 5 and 6 were excluded from further interpretation due to deviation from replicates EXP3 and EXP4, respectively.**

	<b>BoT (mOhm)</b>	<b>EoT (mOhm)</b>	<b>Change (mOhm)</b>	<b>Change (%)</b>
<b>EXP1</b>	8.01	8.40	0.40	5.0
<b>EXP2</b>	7.27	9.06	1.79	24.6
<b>EXP3</b>	6.77	7.34	0.56	8.3
<b>EXP4</b>	6.50	10.05	3.55	54.7
<b>EXP5*</b>	23.60	24.13	0.52	2.2
<b>EXP6*</b>	23.00	32.72	9.71	42.2
<b>AVG 1-4</b>	7.14		1.58	
<b>SD 1-4</b>	0.63			
<b>RSD (%)</b>	8.8			

The segmented fuel cell fixture was found to have much higher impedance than the conventional cell fixtures. Experiments 5 and 6 were, thus, excluded from further interpretation due to deviation from replicates EXP3 and EXP4, respectively. The variance in initial cell resistance was calculated for EXP1-EXP4 and found to be 8.8 %. The relative change in impedance for EXP5 and EXP6 was expected to be comparable to those of the other experiments.

Based on the changes in cell resistance, main effects of Temperature, Relative Humidity and Current Density were calculated. The results are shown in Table 13.

**Table 13. Calculation of main effects based on EIS data. All numbers in mOhm.**

<b>Variable</b>	<b>Interaction</b>	<b>Average High</b>	<b>Average Low</b>	<b>Main Effect</b>
<b>T</b>	RHxJ	3.6	1.1	2.5
<b>RH</b>	TxJ	4.2	0.5	3.7
<b>J</b>	TxRH	1.2	3.5	-2.3
<b>AVG</b>				2.3

For all experiments, an average increase in cell resistance was found to be 2.3 mOhm. At a current level of 10 A (0,4 Acm<sup>-2</sup>), this amounts to a voltage loss of 23 mV. Assuming a nominal cell voltage of 700 mV and an acceptable voltage degradation of 10 %, this means that the performance loss due to the increased ohmic cell resistance is substantial.

The contrast between experiments performed at high versus low temperature shows that temperature contributes to the increase in cell resistance. This is even more pronounced for relative humidity where the largest effect is found. This may be explained by an increase in membrane contamination by impurities introduced by water in the humidified gases. Current density is seen to have the opposite effect; increasing the current density reduces the cell resistance. The reason for this effect is not well understood, but might be associated with the magnitude of transport of impurities and dissolved Pt from the cathode. If Pt-ions play a role in this context, the increased current density causing higher electro-osmotic drag (water transport from anode to cathode) allowing fewer Pt<sup>2+</sup> ions to enter the membrane.

### 2.3.3 Other AST protocols with insufficient data for statistical analyses

#### Reformat operation

The two experiments performed do not comprise a fundament for statistical evaluation of the effect of running reformat instead of hydrogen.

#### Dead-End operation

Experiments under the Dead-End AST protocol was performed by SINTEF using a reference state-of-the-art MEA from Gore as well as a MEA from IRD/FumaTech manufactured within the KeePEMalive project. For the Gore MEA, SINTEF found no significant degradation after 250 hours of operation. For the IRD/FumaTech MEA, two tests were carried out. These tests lasted 132 and 72 hours, respectively. It was found that the Fuel Cell Technology fuel cell fixture was not compatible with the F-940 membrane applied, as the o-ring sealing caused rupture near the edge of the MEA active area. TUG performed experiments with the same IRD/FumaTech membrane without observing membrane rupture. Although CO<sub>2</sub> evolution was observed, significant performance degradation was not found.

#### Start-Stop Cycling

One test has been conducted with a reference, state-of-the-art MEA from Gore. The test gave evidence of a high degradation rate, -3.7 mV h<sup>-1</sup>, and the test was terminated after 110 hours. It was concluded that the number of start and stops executed is the main driving force for the high degradation rate. During the revision of the AST protocols, it was decided to discontinue this protocol. Hence, the data has not been further evaluated.

#### Load Cycling

For the Load Cycling AST protocol, four experiments have been performed by both EIFER (cycling between 200 and 600 mA cm<sup>-2</sup>) and FumaTech (cycling between 0 and 400 mA cm<sup>-2</sup>). Neither set provide data for statistical evaluation and calculation of effects.

From EIFER it was found that degradation rates were low for experiments conducted at 65 °C. This was also the case when the relative humidity was 0 %. The two experiments performed at 85 °C were stopped early due to fuel cell failure.

From the experiments performed by FumaTech, it was concluded that load cycling could not be performed at 0% RH, neither at 65 nor 85 °C. The effect of load cycling including OCV conditions was shown to have only moderate effect on voltage degradation.

## 2.4 Summary and conclusions on main factors causing degradation

It is a general observation that performance degradation rates increase with higher temperature. This is statistically shown for the fuel starvation protocol, where only temperature was shown to have significant impact on the test duration (number of starvation cycles executed). Also, when evaluating the performance decay, temperature has a large impact. Statistical evaluation shows that the effects of relative humidity and current are also significant. Here, the effect of temperature seems to be stronger for characterization in the mass polarization range of the UI curve.

Low (0%) relative humidity has been shown by the load cycling protocol to have detrimental effect on fuel cell performance, even on low temperature setting.

By applying a start/stop protocol, with air purging of the anode, a high degradation rate was observed in one experiment conducted.

Statistical analysis of the experiments performed under the fuel starvation protocol indicates that a significant loss of performance is due to increased cell resistance. Cell temperature and relative humidity contributes to this increase while the current density level of the experiment counteracts the increase in resistance. The losses of ECSA, extrapolated to 400 hours of testing were found to be as large as 50%. The losses could not be specifically ascribed to any of the test input parameters.

The application of load cycling with excursions to OCV was not shown to have as high impact on performance degradation as expected.

In general it can be concluded that the degradation rates are higher at higher current densities for a given cell. This indicates that diffusion (mass transfer) limitations are experienced and limiting the performance at high current densities. This may be linked to changes in the gas diffusion layers (GDLs) and should be explicitly examined in the further work in WP3. More specifically: whereas the effects of Relative Humidity and Current Density appear to be fairly constant over the polarization curve for the Fuel Starvation AST protocol, this is not the case for temperature. From current densities ranging from 50 to 600 mA cm<sup>-2</sup>, the effect of temperature on the degradation rate is more than doubled. This may indicate that Temperature is the main factor inducing material changes in the morphology (hydrophobicity/hydrophilicity) of the Gas Diffusion Layer. Whether this is linked directly to carbon corrosion in the GDL or in the catalyst layer is yet to be determined.

### 3 Modelling of *ex-situ* catalyst degradation

#### 3.1 Introduction

In addition to the extensive *In-situ* ASTs described in Section 2 *Ex-situ* characterization of materials has been conducted within the framework of the *KeePEMalive* project. These include catalyst degradation tests performed in WP 3 by electrochemical cycling. This chapter describes the adaption of a mathematical model to experimental *ex-situ* catalyst degradation tests.

#### 3.2 Experimental conditions and results from catalyst degradation experiments

For a 65 wt% Pt/C catalyst from CABOT, the loss of electrochemical active surface area (ECSA), determined from cyclic voltammograms, was studied under various degradation protocols. These included cycling between 0.9 and 1.2 V, denoted the "Start-Up" (SU) protocol, cycling between 0.6 and 0.9 V, the LOAD protocol, as well as cycling between 0.6 and 1.2 V, the so-called "Shut Down protocol" (SD). The experiments were carried out at room temperature in an air-saturated electrolyte (0.5 M H<sub>2</sub>SO<sub>4</sub>), at two different rates, 100 mV/s and 800 mV/s. Further details regarding these experiments are provided in the *KeePEMalive* deliverable report D3.3<sup>9</sup> [1]. Figure 21 shows a comparison of the relative loss of ECSA, after 6k, 12k and 18k cycles, respectively. The notation indicate the protocol used (SU, LOAD and SD), as well as the cycling rate (100 or 800 mV/s). Some experiments were conducted with squared wave cycles, these are denoted "swc". Triangular cycling was the default.

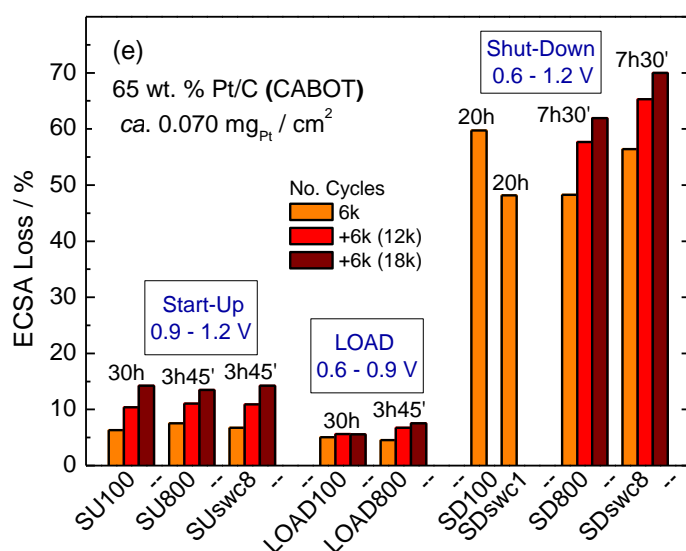


Figure 21. Comparison of ECSA loss for CABOT catalyst cycled according to Start-Up protocol, LOAD protocol and Start-Up Shut Down protocol, at 6k, 12k and 18k cycles.

Some characteristic features of these results are summarized below:

- Start-up conditions (SU), implying cycling between 0.9 and 1.2 V, is more detrimental than cycling between 0.6 and 0.9 V (referred to as LOAD conditions).
- For the SU protocol, degradation rate increases by almost one order of magnitude upon increasing the cycling rate from 100 mV/s to 800 mV/s
- For the SU protocol, triangular and square wave cycling gives similar results

<sup>9</sup> D. Jones, L. Colmenares, Report D3.3: "Ex situ characterization data MEA/stack components", *KeePEMalive* project.

- For the LOAD protocol at 100 mV/s, the degradation saturates already after 6k cycles
- For the LOAD protocol, increasing the cycling rate to 800 mV/s leads to a significant increase in the degradation rate (about one order of magnitude), and the effect is more severe than for the SU protocol. Furthermore, the apparent "saturation" of ECSA loss, as observed for 100 mV/s, vanishes.
- The most detrimental protocol appears to be the Shut Down (SD) protocol (0.6-1.2 V).
- For the SD protocol, increasing the cycling rate from 100 mV/s to 800 mV/s increases the degradation by more than 60%.
- For the SD protocol, degradation differs for triangular cycles and square wave cycles. Triangular cycles are most detrimental at a rate of 100 mV/s, whereas square wave cycles are most detrimental at 800 mV.

### 3.3 Mathematical model

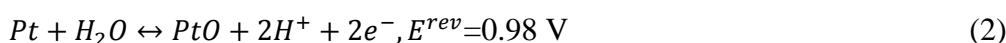
In recent works by Rinaldo *et. al.*<sup>10</sup>, as well as Darling and Meyers<sup>11</sup>, mathematical models for catalyst degradation mechanisms, like chemical dissolution of PtO and electrochemical dissolution of Pt, are provided. These are briefly reviewed below.

At low potentials (vs. SHE), electrochemical dissolution of Pt, according to



will be the dominating degradation mechanism.

At higher potentials, formation of Pt oxides occurs, which may be described as:



The subsequent chemical dissolution of PtO, may, in its simplest form, be described as:



However, as stated in Ref. 10, the exact nature of the oxide is not known, and may vary in the various potential regimes. There are several reactions suggested in the literature, including dissolution of PtO<sub>2</sub>, PtOH and Pt(OH)<sub>2</sub>.

The model by Rinaldo *et. al.* takes into account the evolution of the particle size distribution in time according to the following continuity equation in the particle space:

$$\frac{\partial f(r,z,t)}{\partial t} + \frac{\partial}{\partial r} \left[ \frac{dr}{dt} f(r,z,t) \right] = 0 \quad (4)$$

where  $f(r,z,t)$  is the particle radius distribution, defined as the number of particles per unit volume at time  $t$  with radius in the range from  $r$  to  $r+dr$ .

The models presented in Refs. 10 and 11 also takes into account particle size effects through the Gibbs-Thompson relation<sup>12</sup>, assuming that the chemical potential per metal atom as a function of particle radius  $r$  is given as:

$$\mu(r) = \mu(\infty) + \frac{2\gamma_{Pt}\bar{V}_{Pt}}{r} \quad (5)$$

where  $\mu(\infty)$  is the chemical potential of the bulk metal phase,  $\gamma_{Pt}$  is the interfacial surface tension, and  $\bar{V}_{Pt}$  is the molar volume of the bulk metal.

<sup>10</sup> S.G. Rinaldo, J. Stumper, M. Eikerling, "Physical Theory of Platinum Nanoparticle Dissolution in Polymer Electrolyte Fuel Cells", J. Phys. Chem., 114 (2010) 5773.

<sup>11</sup> R.M. Darling and J. P. Meyers, J. Electrochem. Soc., 150 (2003) A1523.

<sup>12</sup> W. Plieth, J. Phys. Chem., 86 (1982) 3166.

Equation (5) is incorporated into the rate constants by incorporation of the  $r^{-1}$  term in the Gibbs energy [2]:

$$k(r) = k^{\infty} \exp\left(-\frac{\Delta G^{\infty}}{RT} + \frac{2\beta\gamma_{Pt}\bar{V}_{Pt}}{RT r}\right) \quad (6)$$

where  $\Delta G^{\infty}$  is the Gibbs energy of a particle of infinite size,  $k^{\infty}$  is the pre-exponential factor, and  $\beta$  is a proportionality constant. Equation (6) is important to understand the dependence of dissolution rate on particle size.

In Ref. 10, a simplified, analytical solution of the loss of ECSA is provided, valid under the following assumptions: i) The oxide coverage is close to 1 ii) The Pt-ion concentration in the solution is low, iii) there is no spatial variation of concentrations or potential within the catalyst layer. Under these conditions, the dissolution of Pt-O is the dominant degradation mechanism, occurring at a rate of

$$k_3 = k_3^{\infty} \exp\left(\frac{2\beta\gamma_{Pt}\bar{V}_{Pt}}{RT r}\right) \theta_{PtO} \left(\frac{c_{H^+}}{c_{H^+}^{ref}}\right) \left(\frac{c_{O_2}}{c_{O_2}^{ref}}\right) \quad (6)$$

and with the corresponding change of particle size given as:

$$\frac{dr}{dt} = -\bar{V}_{Pt} k_3 \quad (7)$$

Rinaldo *et al* [ref. 10] show that by combining equations (4), (6) and (7), an implicit solution to the problem can be derived, given by

$$f(\xi, \tau) = f_0(\xi_0) \exp(-(\xi - \xi_0)) \quad (8)$$

for the new particle size distribution, with  $f_0(\xi_0)$  as the original particle size distribution.

The non-dimensional variables

$$\tau = \frac{t}{T} \text{ and } \xi = \frac{R_0}{r}$$

have been introduced. Characteristic time and radius are defined by

$$T_0 = \frac{2\beta\gamma_{Pt}\bar{V}_{Pt}}{RT r_3} \text{ and } R_0 = \frac{2\beta\gamma_{Pt}\bar{V}_{Pt}}{RT}$$

The following implicit solution allows for the determination of the new particle size after elapse of the time  $t$  ( $\tau$ ):

$$-\frac{\exp(-\xi)}{\xi} + Ei(\xi) = \tau - \frac{\exp(-\xi_0)}{\xi_0} + Ei(\xi_0) \quad (9)$$

where  $Ei(\xi)$  is the exponential integral of  $\xi$ .

### 3.4 Adaption of the mathematical model to the experimental results

The model for change in ECSA due to dissolution of oxide, as described by Rinaldo *et al* [ref. 10] (equations 8 and 9) was applied to the experimental data obtained for the SU protocol, shown in Figure 22. In the potential range 0.9-1.2 V (vs. SHE), it seems reasonable to assume that chemical dissolution of PtO is the predominant degradation mechanisms, as the Pt surface coverage may be assumed to be close to 1. This is confirmed by the theoretical calculations performed by Darling and Meyers [ref. 11], as shown in Figure 22. Here, the oxide coverage at a cycling rate of 100 mV was obtained by fitting their model for oxide formation to experimental data. As can be seen from Figure 22, the estimated oxide coverage is close to 1 for potentials > 0.9 V. Also, upon reduction of the potential from 1.2 V, there is a kinetic limitation causing the oxide coverage to remain at a high value for potentials > 0.8 V.

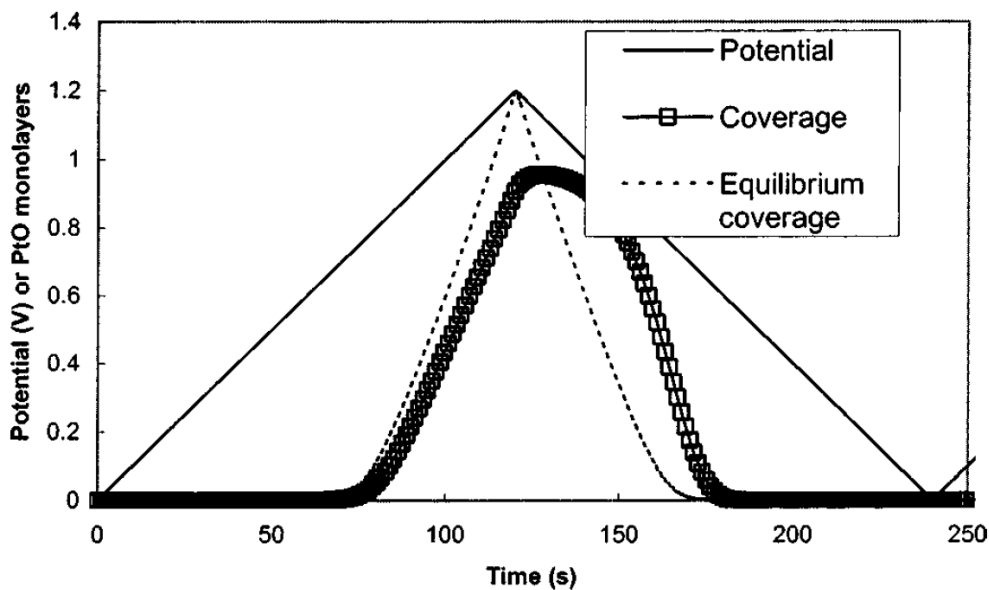


Figure 22. Theoretical calculation of the PtO coverage of a Pt catalyst subject to potential cycling at a rate of 100 mV/s [3].

For the CABOT catalyst tested within Keepemalive, the exact initial particle size distribution is not known, but as stated in ref. 9, the mean particle size is 2.9 nm, with a negligible amount of particles below 2.8 nm, or above 4.0 nm. Based on this information, the particle size distribution depicted in Figure 23 was constructed, and assumed as the initial distribution.

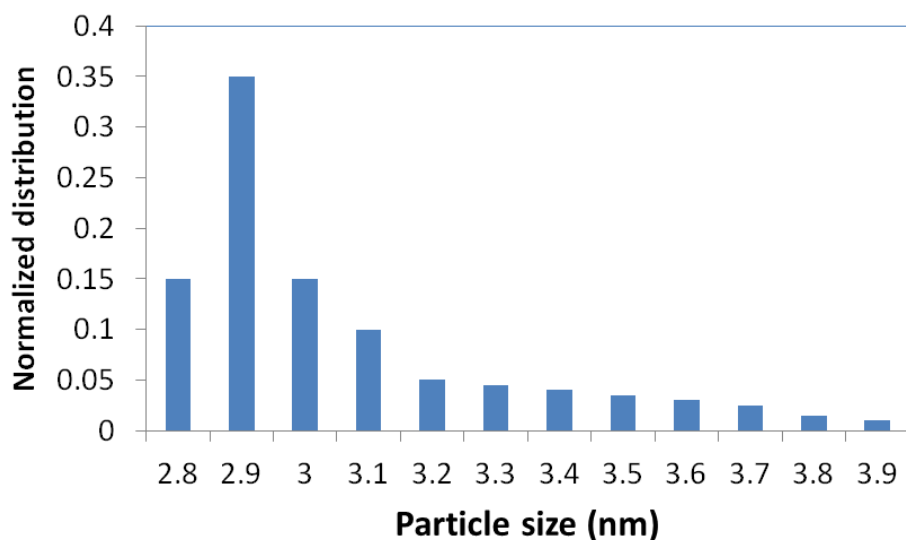
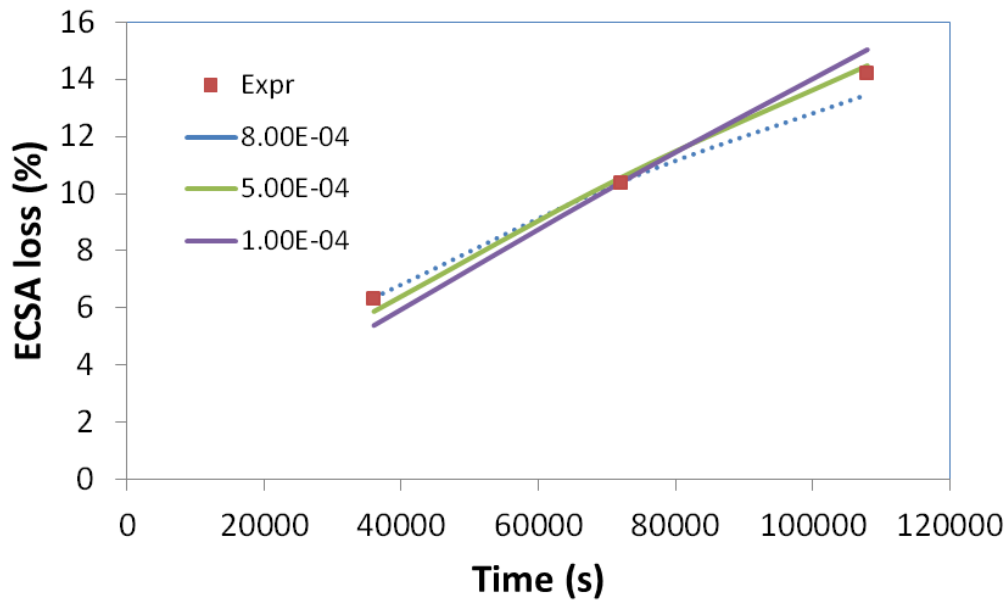


Figure 23. Assumed initial particle size distribution (normalized).

When fitting the experimental data (Figure 21) to the model, a value for the parameter  $\beta\overline{V}_{Pt}$  was selected first, and then the rate constant was adjusted in order to obtain the best fit to the experimental data. For low values of  $\beta\overline{V}_{Pt}$ , the estimated loss of ECSA is linear in time, whereas a too high value causes a too high deflection of the relative ECSA loss. Figure 24 shows the experimental results for the SU protocol at a rate of 100 mV/s compared to model results obtained for various values of  $\beta\overline{V}_{Pt}$  ( $8e^{-4}$ ,  $5e^{-4}$ , and  $1e^{-4}$  J/cm<sup>2</sup>, as indicated in the legend). As is seen from Figure 24,  $\beta\overline{V}_{Pt} = 5e^{-4}$  J/cm<sup>2</sup> appears to give the best fit, together with the rate constant  $k_3 = 3.95e^{-9}$  mol/cm<sup>2</sup> s.



**Figure 24.** Fitting of the oxide dissolution model to the experimental data for the SU protocol, for various values of  $\beta\overline{V}_{Pt}$  (as indicated in the legend).

For the SU protocol, the data obtained at 800 mV/s were fitted in the same manner. The value of  $\beta\overline{V}_{Pt}$  may be assumed to be independent of cycling rate, thus the value found to give the best fit in Figure 24 was chosen ( $5.0 \times 10^{-4} \text{ J/cm}^2$ ), and the rate constant adjusted to  $k_3 = 3.3 \times 10^{-8} \text{ mol/cm}^2 \text{ s}$ .

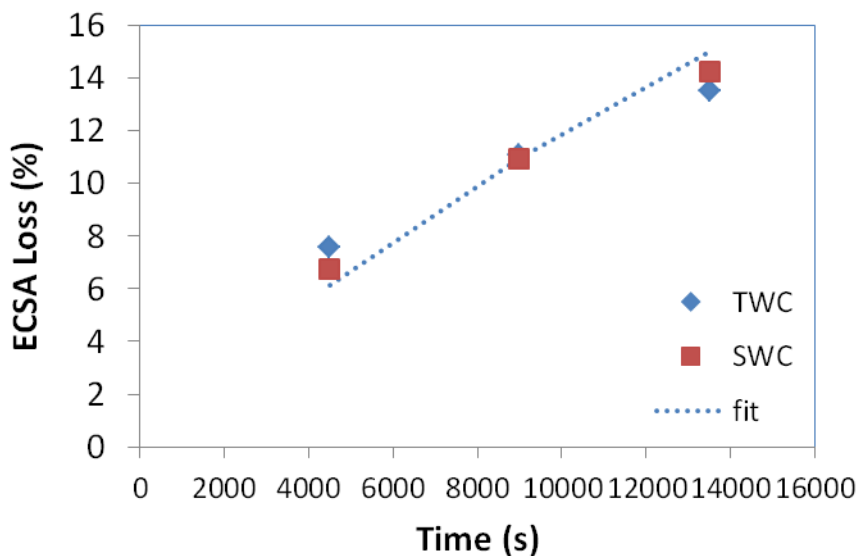


**Figure 25.** Fitting of the oxide dissolution model to the experimental data for the SU protocol at 800 mV/s, for  $\beta\overline{V}_{Pt} = 5.0 \times 10^{-4} \text{ J/cm}^2$  and  $k_3 = 3.3 \times 10^{-8} \text{ mol/cm}^2 \text{ s}$ .

Equation (6) provides an explanation for the dependence of degradation rate on the cycling rate. As rapid cycling will facilitate mass transfer of the reactants to the reaction sites, the terms

$$\left(\frac{c_{H^+}}{c_{H^+}^{ref}}\right)\left(\frac{c_{O_2}}{c_{O_2}^{ref}}\right)$$

in equation (6) will be higher. Thus, a higher rate constant is expected during rapid cycling, causing an increased degradation rate.

For the SU protocol, no dependence on the type of cycles (triangular or squared) is seen. This supports the conclusion that the degradation rate is dominated by PtO dissolution.

For the LOAD and SD protocols, full oxide coverage throughout the entire cycle cannot be assumed. Potential hold experiments or cycling at potentials below 0.8 V, indicate that degradation rates are low in these potential regimes. Thus, it seems reasonable to assume that the degradation observed during the LOAD protocol to a large extent is related to dissolution of PtO for the periods of the cycle when the potential is > 0.8 V. During the load cycle, re-oxidation of bare Pt might also occur. The large effect of increasing the cycling rate to 800 mV/s may be understood using the same arguments as above, namely that improved mass transfer leads to an increase in the rate constant. In addition, in view of the results obtained in Ref. 11, and shown in Figure 22, it is likely that rapid cycling leads to a higher average coverage during one cycle, since slow kinetics retards the stripping of the oxide even more at 800 mV/s.

The PtO dissolution model cannot predict the apparent "saturation" of the degradation, as observed for the LOAD protocol at 100 mV/s.

The arguments provided above would also apply for the SD protocol, where the oxide coverage will be close to 1 during a significant fraction of the cycle. For the SD protocol, it therefore appears reasonable that the cycling mode (twc or swc) affects the degradation, as it will influence on the oxide coverage (ref. Figure 22). Obviously, oxidation and re-oxidation are more severe for this protocol.

A more accurate description of the degradation of the LOAD and SD protocol will need to include a mass balance for Pt<sup>2+</sup> and PtO.

### 3.5 Conclusion

Dissolution of PtO appears to be the major degradation mechanism of Pt/C catalyst under "normal" operating conditions.

## 4 Input to revision of the AST program

Several important aspects of fuel cell testing by experimental design have been assessed and these are described in Chapter 1 through 3. By evaluating the initial variance of several characterization parameters (i.e., cell voltage, cell resistance, ECSA) better understanding of the magnitude of the effects on degradation required in order to be significant has been obtained.

Several of the characterization techniques applied indicates that the break-in procedure applied does not lead to peak performance at BoT. This implies that a combination of performance gain as well as degradation is registered in the subsequent characterization. It is therefore difficult to evaluate degradation specifically as performance increase due to insufficient break-in masks the initial cell degradation. This has been remedied by introducing voltage cycling in the revised AST protocols (Figure 26).

While the statistical evaluation of fractional factorial (e.g.,  $2^{3-1} = 4$ ) experiments can be useful for screening purposes, full sets of  $2^3$  experiments should be executed in order to be able to separate main effects from interactions. While less labour would be required in completing the AST experiments already carried out as part of the first phase of the AST program, the in-sufficient break in for these experiments linked to changes in fuel cell components (new reinforced membranes introduced in the project) suggest that new complete set of factorial experiments are required.

Problems encountered during the first phase of the AST program included instable operation at certain combination of experimental conditions, leaving 4 out of 6 sets of data from AST protocols inadequate for further statistical analyses. Thus, to remedy this in phase 2 of the AST program, parameter verification experiment will constitute the start for all new ASTs. In these verification experiments all combinations of experimental conditions for that AST are evaluated prior to launching long term experiments to ensure that stable operation may be achieved. In this way, the failure to complete AST experiments can be avoided. To exemplify this, the load and set points profiles for the revised Continuous Operation AST are illustrated in Figure 26.

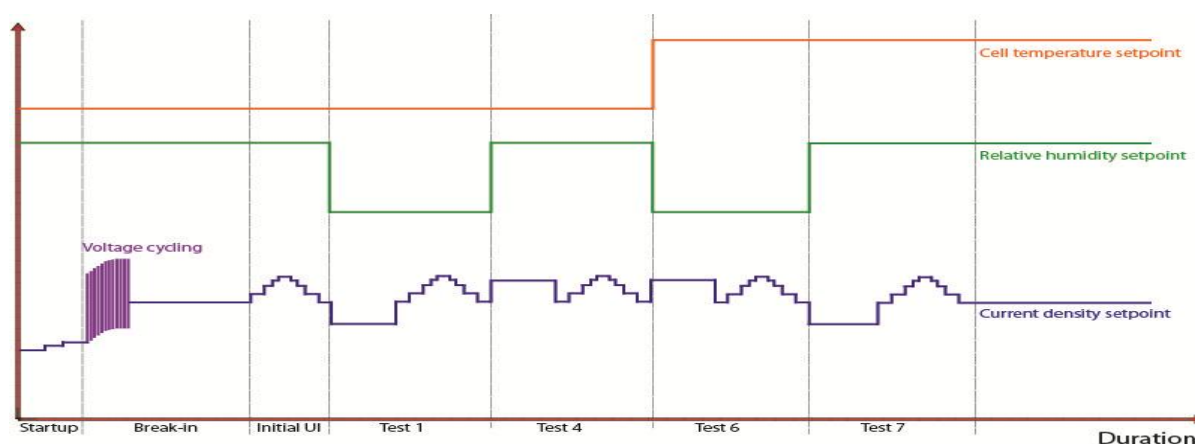


**Figure 26. Example of a parameter verification experiment for four out of eight experiments for the Continuous operation AST.**

Based on ex situ catalyst characterization, the modelling efforts of catalyst degradation suggest that PtO is involved in the dissolution of the catalyst. Therefore, ex situ characterization should put emphasis on how to better confirm the role of PtO in the degradation of the catalyst under specific applied potential cycling profile.

## 5 Abbreviations

AST	<u>A</u> ccelerated <u>S</u> tress <u>T</u> est
BoL	<u>B</u> eginning- <u>o</u> f- <u>L</u> ife
BoP	<u>B</u> alance- <u>o</u> f- <u>P</u> lant
BoT	<u>B</u> eginning- <u>o</u> f- <u>T</u> est
CV	<u>C</u> yclic <u>V</u> oltammogram
CVMS	<u>C</u> ell <u>V</u> oltage <u>M</u> onitoring <u>S</u> ystem
ECSA	<u>E</u> lectro <u>C</u> hemical <u>S</u> urface <u>A</u> rea
EIS	Electrochemical Impedance Spectroscopy
EoL	<u>E</u> nd- <u>o</u> f- <u>L</u> ife
EoT	<u>E</u> nd- <u>o</u> f- <u>T</u> est
EXP	<u>E</u> xperiment
FC	<u>F</u> uel <u>C</u> ell
GDL	<u>G</u> as <u>D</u> iffusion <u>L</u> ayer
LT	<u>L</u> ow <u>T</u> emperature
LTS	<u>L</u> ow <u>T</u> emperature gas <u>S</u> hift
J	Current Density
MEA	<u>M</u> embrane <u>E</u> lectrode <u>A</u> ssemblies
μCHP	Micro Combined Heat and Power
OCV	<u>O</u> pen <u>C</u> ell <u>V</u> oltage
PEM	<u>P</u> roton <u>E</u> xchangeable <u>M</u> embrane
RH	<u>R</u> elative <u>H</u> umidity
RSD	<u>R</u> elative <u>S</u> tandard <u>D</u> eviation
SD	<u>S</u> hut <u>D</u> own
SU	<u>S</u> tart <u>U</u> p
T	<u>T</u> emperature
VPP	<u>V</u> irtual <u>P</u> ower <u>P</u> lant